The Astrophysical Journal, 770:58 (17pp), 2013 June 10 doi:10.1088/0004-637X/770/1/58

CANDELS OBSERVATIONS OF THE ENVIRONMENTAL DEPENDENCE OF THE COLOR–MASS–MORPHOLOGY RELATION AT $z = 1.6$

Robert Bassett[1,2,9], Casey Papovich[1,2], Jennifer M. Lotz[3], Eric F. Bell[4], Steven L. Finkelstein[5,14], Jeffrey A. Newman[6], Kim-Vy Tran[1,2], Omar Almaini[7], Caterina Lani[7], Michael Cooper[8,14], Darren Croton[9], Avishai Dekel[10], Henry C. Ferguson[3], Dale D. Kocevski[11], Anton M. Koekemoer[3], David C. Koo[11], Elizabeth J. McGrath[11], Daniel H. McIntosh[12], and Risa Wechsler[13]

[1] George P. and Cynthia Woods Mitchell Institute for Fundamental Physics and Astronomy, College Station, TX 77843-4242, USA
[2] Department of Physics and Astronomy, Texas A&M University, College Station, TX 77843-4242, USA
[3] Space Telescope Science Institute, 3700 San Martin Dr., Baltimore, MD 21218, USA
[4] Department of Astronomy, University of Michigan, Ann Arbor, MI 48109, USA
[5] Department of Astronomy, University of Texas, Austin, TX 78712, USA
[6] Department of Physics and Astronomy, University of Pittsburgh, Pittsburgh, PA 15260, USA
[7] School of Physics and Astronomy, University of Nottingham, Nottingham, UK
[8] Center for Galaxy Evolution, Department of Physics and Astronomy, University of California, Irvine, 4129 Frederick Reines Hall, Irvine, CA 92697, USA
[9] Centre for Astrophysics and Supercomputing, Swinburne University of Technology, Hawthorn, Australia
[10] Racah Institute of Physics, The Hebrew University, Jerusalem 91904, Israel
[11] UCO/Lick Observatory, Department of Astronomy and Astrophysics, University of California, Santa Cruz, CA 95064, USA
[12] Department of Physics, University of Missouri-Kansas City, 5110 Rockhill Road, Kansas City, MO 64110, USA
[13] Kavli Institute for Particle Astrophysics and Cosmology, Physics Department, and SLAC National Accelerator Laboratory, Stanford University, Stanford, CA 94305, USA
Received 2012 May 10; accepted 2013 April 28; published 2013 May 24

ABSTRACT

We study the environmental dependence of color, stellar mass, and morphology by comparing galaxies in a forming cluster to those in the field at $z = 1.6$ with *Hubble Space Telescope* near-infrared imaging in the CANDELS/UDS field. We quantify the morphology of the galaxies using the effective radius, $r_{\rm eff}$, and Sérsic index, n. In both the cluster and field, approximately half of the bulge-dominated galaxies ($n > 2$) reside on the red sequence of the color–magnitude diagram, and most disk-dominated galaxies ($n < 2$) have colors expected for star-forming galaxies. There is weak evidence that cluster galaxies have redder rest-frame $U - B$ colors and higher stellar masses compared to the field. Star-forming galaxies in both the cluster and field show no significant differences in their morphologies. In contrast, there is evidence that quiescent galaxies in the cluster have larger median effective radii and smaller Sérsic indices compared to the field with a significance of 2σ. These differences are most pronounced for galaxies at clustercentric distances 1 Mpc $< R_{\rm proj} <$ 1.5 Mpc, which have low Sérsic indices and possibly larger effective radii, more consistent with star-forming galaxies at this epoch and in contrast to other quiescent galaxies. We argue that star-forming galaxies are processed under the influence of the cluster environment at distances greater than the cluster-halo virial radius. Our results are consistent with models where gas accretion onto these galaxies is suppressed from processes associated with the cluster environment.

Key words: galaxies: clusters: general – galaxies: evolution – galaxies: high-redshift – galaxies: structure

Online-only material: color figures

1. INTRODUCTION

Galaxies in the low redshift universe show a very strong dependence between environment, morphology, color, and stellar mass (e.g., Hogg et al. 2004; Kauffmann et al. 2004; Skibba et al. 2009). Galaxies in regions of higher local density, such as galaxy groups and clusters, have lower levels of star formation, higher fractions of red, passive galaxies, and more early-type morphologies compared to galaxies in lower local number density regions (e.g., Dressler 1980; Postman & Geller 1984). Poggianti et al. (2008, and others) find that this relation extends to intermediate redshifts ($z \sim 0.4$–0.8) with the highest density regions being exclusively populated by elliptical morphological types.

It is difficult, however, to separate the galaxy properties which depend on high local density (regions of dense "environment") from those which depend on galaxy mass. One challenge is that galaxies in regions of high local density have higher average halo and stellar masses, and care must be taken to study environmental effects on samples at fixed stellar mass. For example, Kauffmann et al. (2004) showed that the red, passive galaxies at $z \sim 0.1$ that dominate in high local density regions have highly concentrated morphologies, but at fixed mass their sizes and concentrations are almost independent of environment. Guo et al. (2009) find that the concentrations of the central galaxies of dark matter halos at $0 \lesssim z \leqslant 0.2$ depend strongly on their stellar mass, but only weakly on their halo mass, implying a weak dependence on environment. Similarly, van der Wel (2008) show that galaxies at $z \sim 0.02$ with the highest masses show no dependence between morphological concentration and environment (local density of galaxies). It is only for lower mass galaxies ($M \sim 3 \times 10^{10}$–$5 \times 10^{10}\,M_{\odot}$) that there is a weak trend toward higher galaxy concentration in higher local density regions. Therefore, the environment has a subtle effect on galaxy morphologies at low redshifts.

Grützbauch et al. (2011b) show that these trends persist to higher redshifts ($z \sim 0.4$–1.0) and that the intrinsic properties of a galaxy are more dependent on stellar mass than local

[14] Hubble Fellow.

density at earlier epochs. In a similar redshift range, some studies attempted to disentangle the color–mass–density relation and its evolution by examining the colors or morphologies of galaxies as a function of local density in narrow bins of redshift and stellar mass (Tasca et al. 2009; Cucciati et al. 2010). These studies found that the correlation between color, mass, and density is considerably weaker at higher redshifts with the exception of galaxies in the low mass regime. The implication is that these lower mass galaxies were formed more recently in a time when evolved large-scale structures were already in place.

In contrast, the environment does appear to have a strong effect on the relative star-formation rates (SFRs) of galaxies. Hogg et al. (2003) showed that at $z \sim 0.2$, the density of galaxies correlates with color: redder galaxies lie in regions of higher local density (see also, Blanton et al. 2005; Baldry et al. 2006). Similarly, Kauffmann et al. (2004) found that higher density regions anticorrelate most strongly with galaxy specific SFR (sSFR, the SFR per unit stellar mass): galaxies in high local number density regions have lower average sSFRs. Patel et al. (2009) show that this trend also persists to higher redshifts ($z \sim 0.7$). Interestingly, most of this effect on the sSFRs does not arise from an environmental dependence on the properties of star-forming galaxies, which appear unchanged between regions of high and low local number density (Hansen et al. 2009; Peng et al. 2010; Wetzel et al. 2011). Instead, it is the fraction of quenched galaxies that increases with increasing galaxy density that drives this observation (Peng et al. 2010).

Several authors have argued that this quenching fraction is different for galaxies that are "centrals" or "satellites" in their halos, where quenching in centrals depends primarily on the galaxy's halo mass while the quenched fraction of galaxies that are "satellites" depends on their distance from the halo center (e.g., Wetzel et al. 2011; Wilman et al. 2011; Woo et al. 2012). Hansen et al. (2009) find that the fraction of red (quenched) and blue (star-forming) galaxies changes dramatically with distance from the center of clusters. Wetzel et al. (2011) find that the fraction of quenched galaxies persists out to $\approx 2R_{\rm vir}$, where $R_{\rm vir}$ is the virial radius of the halo (e.g., Hansen et al. 2009). Selecting galaxies in bins of morphological type, Guo et al. (2009) find no evidence that the structures of early-type galaxies differ between central and satellite galaxies matched in both optical color and stellar mass, although Weinmann et al. (2009) find that late-type satellite galaxies show smaller radii and larger concentrations than late-type centrals. Weinmann et al. (2009) also find that late-type satellites have redder colors than late-type central galaxies. This suggests that the stellar mass of the galaxy is the more fundamental property determining the structure of early-type galaxies, and that observed differences in satellite and central galaxies may be due to the quenching of galaxies after they become satellites. Woo et al. (2012) argue that these observations are consistent with theoretical expectations that quenching mechanisms affect the satellites as they move into the environment of the larger mass halo (e.g., Bahe et al. 2012).

It is unclear how these trends between color, SFR, morphology, mass, and environment evolve with redshift. Both Cooper et al. (2007) and Elbaz et al. (2007) observed that the low redshift SFR–density relation evolves and possibly reverses around $z \sim 1$. It has also been observed that at $z \sim 1$–1.6, the surface density of IR-luminous, star-forming galaxies increases in regions of high local density (e.g., Tran et al. 2010; Kocevski et al. 2011). However, the study of Grützbauch et al. (2011a) found that in the redshift range $1 \lesssim z \lesssim 3$ there is a strong dependence between SFR (and sSFR) and stellar mass, and very weak (if any) dependence between SFR and environment (see also, Bauer et al. 2011a). It is only in the highest local number density regions where star formation is significantly suppressed, and this is only apparent to $z \sim 2$. However, studies show that even at these redshifts, regions of high local density contain a dominant population of mostly quiescent galaxies, and the overall trend in color and sSFR remains mostly unchanged from $z \sim 0$ (Cooper et al. 2008; Chuter et al. 2011; Quadri et al. 2012).

Other studies have looked at the relation between galaxy size (morphology) and environment at $z > 1$ (Cooper et al. 2011; Zirm et al. 2011; Papovich et al. 2012). These studies have found that at fixed mass, spheroidal (bulge-dominated, with Sérsic index $n > 2$) galaxies in regions of higher density have larger sizes compared to spheroidal galaxies in low-density regions. This seems to imply that there are processes associated with the higher density regions that enhance or accelerate galaxy growth. One obvious candidate is an apparent higher merger rate for galaxies in higher density environments. Indeed, Lotz et al. (2013) observe an enhancement in the rate of dissipationless (gas poor, or "dry") mergers in galaxies in a forming cluster at $z = 1.62$ compared to similarly selected galaxies in the field (similar to the findings of Tran et al. 2005, at $z = 0.83$). If these "dry" mergers are in fact the dominant driver of the size evolution of early type galaxies, then they may also affect the galaxy morphologies (e.g., Navarro 1990), and we may expect to find variation in galaxy structure at this epoch.

One reason it is difficult to disentangle galaxy evolution effects arising from "environment" from those which depend on "mass" is that different methods are used to define "environment" and these are sensitive to the effects of environments on different scales. Many methods have appeared in the literature, such as fixed aperture and nearest neighbor distances, but it has been shown that there is considerable scatter between them. Muldrew et al. (2012) compare and contrast different environment estimators using mock galaxy samples taken from the Millennium simulation. They found that different methods probe different aspects of the dark matter halos that contain groups and clusters. For example, nearest neighbor statistics better study the internal halo properties and effects of smaller structures such as group-sized halos. The fixed aperture method, on the other hand, is found to be a better probe of the halo as a whole. However, all of these environment statistics are sensitive to errors in galaxy distances (in particular redshift errors), which can be limiting factors in this analysis.

Here, we extend these studies to understand how galaxy color, stellar mass, and morphology depend on environment at $z = 1.6$ using a portion of the data from the UKIRT Infrared Deep Sky Survey–Ultra-Deep Survey (UKIDSS-UDS) field covered with the *Hubble Space Telescope* (*HST*) as part of the Cosmic Assembly Near-infrared Deep Extragalactic Legacy Survey (CANDELS; Grogin et al. 2011; Koekemoer et al. 2011). These data cover one of the largest contiguous fields with WFC3 near-IR imaging. At $z = 1.6$, this field covers both a forming cluster at $z = 1.62$ and galaxies in the field. Therefore, we are able to study galaxies within a single redshift slice in this large field. This allows us to test effects associated with environment over a very large range in local galaxy density, from the rich environment of a forming cluster to the low density field using a highly homogeneous dataset. Furthermore, because we study galaxies from a single dataset with uniform analysis, any bias from systematics affects all galaxies in a similar way. This means

we can make robust (relative) comparisons between galaxies in different environments.

Throughout this paper, we report magnitudes measured relative to the AB system (Oke & Gunn 1983) and we assume cosmological parameters $\Omega_m = 0.3$, $\Omega_\Lambda = 0.7$, and $H_0 = 70$ km s^{-1} Mpc^{-1}, which give an angular diameter distance of 0.508 Mpc arcmin^{-1} (8.47 kpc arcsec^{-1}) for $z = 1.6$. All projected distances are given in physical (proper) distances at $z = 1.6$.

2. DATA

For this paper, we use available datasets that cover the CANDELS UDS field. The available data in this field include *HST*/WFC3 imaging in the F125W and F160W filters from CANDELS over $9.'4 \times 22.'0$ (Grogin et al. 2011; Koekemoer et al. 2011), corresponding to a projected, physical area 4.8 Mpc $\times$ 11.2 Mpc at $z = 1.6$.

Here we used a photometric catalog containing photometry from the UKIDSS-UDS from Williams et al. (2009) covering *BVRIz* from Subaru/SuprimeCam, *JK* from UKIDSS, and deep *Spitzer*/IRAC imaging from the *Spitzer* UDS covering 3.6–8.0 μm. Our catalog is identical to that used in Papovich et al. (2010). In summary, these catalogs reach 5σ limiting magnitudes of $B < 27.7$, $R < 27.1$, $i < 26.8$, $z < 25.5$, $J < 23.9$, and $K < 23.6$ mag in apertures of $1.''75$ diameter. The catalogs are selected in the K band with colors measured in fixed apertures and they include unique aperture corrections for each source defined as the difference between the fixed aperture and total magnitude derived from the K band for that source (see Williams et al. 2009). We used IRAC catalogs with photometry measured in $4''$ diameter apertures, with aperture corrections to total magnitudes as stated in Papovich et al. (2010). We matched the IRAC sources to the optical+IR data within $1''$ radii. The final catalog covers a wavelength baseline of 0.4–8 μm.

We use the photometric redshift catalog from Papovich et al. (2010) derived using EAZY v1.0 Brammer et al. (2008). In summary, we used the default galaxy spectral energy distribution (SED) templates with the default K-band prior based on the luminosity functions of galaxies in a semi-analytic simulation. In addition to photometric redshifts, we measure the full photometric-redshift probability distribution function, $P(z)$, normalized such that $\int P(z)\,dz = 1$ when integrated over all redshifts. As discussed in Papovich et al. (2010), compared to existing spectroscopic redshifts, the best-fit photometric redshifts have uncertainties of $\Delta([z_{\rm sp} - z_{\rm ph}]/[1 + z_{\rm sp}]) = 0.04$ derived from the normalized median absolute deviation (Beers et al. 1990) in the range $1 \leqslant z_{\rm sp} \leqslant 2$ (which includes the redshift-range of interest in this paper).

We use stellar masses, SFRs and sSFRs (the SFR per unit stellar mass), and rest-frame $U-B$ and $U-V$ colors as derived in Papovich et al. (2012). To summarize, we fit the 10-band galaxy photometry with model SEDs with Chabrier initial mass function and solar metallicity using stellar population synthesis models from Bruzual & Charlot (2003), allowing for a range of stellar population age, star-formation history, and dust attenuation using the Calzetti et al. (2000) law. The rest-frame $U-B$ and $U-V$ colors and SFRs are derived using the best-fit models, where we measure the SFR averaged over the prior 100 Myr. We found that the rest-frame colors for galaxies in our sample agree with those independently derived from the best-fitting templates for the photometric redshifts using EAZY with median rest-frame color differences of $\Delta(U-B) = 0.03$ and $\Delta(U-V) = 0.04$ mag with standard deviations $\sigma(\Delta[U-B]) = 0.04$ and $\sigma(\Delta[U-V]) = 0.08$ mag.

We adopt for our galaxy sample the limiting magnitude from the Williams et al. (2009) catalog of $K = 22.9$ mag. This equates approximately to a 10σ detection limit. This magnitude limit for a galaxy at $z = 1.6$ corresponds to a stellar mass of $\approx 2 \times 10^{10}\,M_\odot$, for a solar metallicity stellar population with a maximum mass-to-light ratio (formed in a burst at $z_f = 5$). Galaxies with younger stellar populations will have lower mass-to-light ratios. Therefore, while our sample is "complete" for all galaxies with stellar masses above $\approx 2 \times 10^{10}\,M_\odot$, our sample is sensitive to galaxies with younger stellar populations with stellar masses below this limit. Therefore, our stellar mass limit is "conservative" in the sense that we are sensitive to all galaxies above this mass limit. The choice for this limiting stellar mass is also motivated by our ability to recover accurate morphological information from the *HST*/CANDELS images with GALFIT. Galaxies at the stellar mass limit and with the fiducial stellar population above have magnitudes of m(F125W) = 24 mag, up to which we can recover robust quantitative morphological parameters with accuracies better than 40% (see below, Section 3.1 and the Appendix). We therefore adopt a limiting mass of $2 \times 10^{10}\,M_\odot$ where we are complete for all galaxies, and for which our analysis is robust.

We focus on the subset of the UDS with CANDELS imaging. In addition to the portion of the UDS covered by CANDELS, we find it is useful to include the full UDS dataset when making comparisons not involving size or morphology. This larger data set covers an area of 0.70 deg^2 (as discussed in Williams et al. 2009; Papovich et al. 2012) and is nearly $10\times$ larger in area than the CANDELS field.

As in Papovich et al. (2012), we select galaxies around redshift $z = 1.6$ by defining the integrated photometric redshift probability distribution function, $\mathcal{P}_z \equiv \int P(z)\,dz$ integrated of the redshift range $z = z_{\rm cen} \pm \delta z$ with $z_{\rm cen} = 1.625$ (Papovich et al. 2010, which corresponds to the mean redshift of the cluster in this field) and $\delta z = 0.05 \times (1 + z_{\rm cen})$, which is typical of the photometric redshift 68% confidence limits at this redshift. Here we select all galaxies with $\mathcal{P}_z = 0.4$. As shown in Papovich et al. (2010), this $\mathcal{P}_z$ limit is required to include blue, star-forming galaxies with spectroscopically confirmed redshifts at $z \sim 1.6$, and it includes the red, quiescent galaxies at this redshift. Using a higher $\mathcal{P}_z$ limit restricts the sample more to quiescent galaxies (as was used by Papovich et al. 2012). Selecting galaxies this way has the advantage that it uses all information about the galaxies' photometric redshift probability distribution functions. In contrast, using samples of galaxies selected solely with a best-fit photometric redshift excludes information, and galaxies selected in some redshift interval will be very dependent on the errors in the photometric redshifts and subject to biases. Regardless, in the case here, we compare the properties of both cluster and field galaxy samples constructed from the same photometric-redshift selection and using the same CANDELS data set. Therefore, any systematics or biases resulting from the selection affect both samples equally. As a result, the relative comparison between the galaxies in the cluster and field is robust.

We select all galaxies with $\mathcal{P}_z > 0.4$. This selection provides a sample of 433 galaxies with coverage in CANDELS imaging with mean (best-fit photometric) redshift $\bar{z} = 1.61$ with a standard deviation of 0.12.

3. ANALYSIS

3.1. Quantifying Galaxy Morphologies

We used GALFIT (Peng et al. 2002) to fit parametric models to the surface brightness profiles of our sample galaxies in the WFC3 F125W imaging. We chose the F125W bandpass for this analysis because it corresponds approximately to the *B* band in the rest-frame at $z = 1.6$. Many studies of the morphologies of distant galaxies (especially in clusters) are based in the rest-frame *B* band (see, e.g., Blakeslee et al. 2003, 2006; Homeier et al. 2005; Postman et al. 2005; Holden et al. 2005; Mei et al. 2009; Santos et al. 2009), and our choice of the F125W bandpass here allows for direct comparisons with these other studies. In addition, the CANDELS imaging allows for studies of galaxy morphology in the rest-frame *B* band out to $z \sim 3$ using the F160W bandpass, which would permit the extension of our work to higher redshift. Therefore our choice here seems prudent. Regardless, our tests (see below) show that none of our conclusions would be changed if we used the F160W bandpass instead.

GALFIT models the surface brightness profile of a galaxy as $\exp(-R/R_{\rm eff})^{1/n}$ (Sersic 1968), where $n = 1$ corresponds to a exponential (disk) profile and $n = 4$ corresponds to the de Vaucouleur's profile. GALFIT convolves these models with a user-defined point spread function (PSF). We used a PSF constructed using TinyTim v7.2 (Krist 1995) and combined with the same dither positions as the CANDELS data. For each galaxy we fit with GALFIT the effective semimajor axis ($a_{\rm eff}$), background, axis ratio (b/a), total magnitude, and Sérsic indices (n) as free parameters.

We compared our Sérsic index measures using the F125W imaging for the galaxies in our $z \sim 1.6$ sample against independent measurements derived using GALAPAGOS (Barden et al. 2012) with the CANDELS WFC3/F160W imaging as described by Bell et al. (2012) and van der Wel et al. (2012). We find a median offset in Sérsic index of -0.03 dex in $\Delta(n)/n$ with a scatter of 0.12 dex and we find a median offset in effective radius of 0.01 in $\Delta(r_{\rm eff})/r_{\rm eff}$ with a scatter of 0.06 dex. The uncertainties are nearly independent of galaxy magnitude, with only minor improvement for $J < 23$ mag compared to $23 < J < 24$ mag. Because these differences are small, our conclusions would be unchanged if we used fits from the F160W imaging instead of the F125W imaging.

We performed a series of simulations, inserting model galaxies into the *HST* data, and using GALFIT as described above to recover their parameters. Our analysis of these simulations showed that the recovered effective radii are accurate to better than 40% and the Sérsic indices to better than 25% for galaxies with $r_{\rm eff} = 2$ kpc and $n = 4$ with magnitude $m({\rm F125W}) = 24$ mag, near the stellar-mass limit of our sample ($2 \times 10^{10}\,M_{\odot}$, see Section 2). Galaxies with parameters such as these represent the worst case scenario, and errors for most objects will be significantly smaller than this. The uncertainties are correlated between parameters, similar to the findings of Häussler et al. (2007). For more information, see the Appendix.

3.2. Quantifying Galaxy Environment

We tested different ways to characterize the environment of each galaxy in our $z = 1.6$ sample. We found that using samples based on the projected distance from the cluster center provided the most significant results. For this reason, we defined two samples. We selected a sample of "cluster" galaxies with $\mathcal{P}_z > 0.4$ and projected distances $R_{\rm proj} < 1.5$ Mpc of the cluster center (with the cluster center defined by Papovich et al. 2010). A subsample of "field" galaxies with $R_{\rm proj} > 3$ Mpc was selected for comparison.

We also calculated environment measures based on the projected distance to the *N*th nearest neighbor, D_N (e.g., Dressler 1980). We computed the *N*th nearest neighbor distance from each galaxy in our $\mathcal{P}_z > 0.4$, $z \sim 1.6$ sample to (1) each other galaxy in the $z \sim 1.6$, $\mathcal{P}_z > 0.4$ sample, as well as to (2) each galaxy in a sample that have *best-fit* photometric redshifts $1.50 < z < 1.75$. Additionally, we tested the *N*th nearest neighbor distance with the requirement that the stellar-mass ratio between each galaxy and its neighbors be greater than or equal to a certain value over a range from 1:1 to 1:10 (as proposed by Haas et al. 2011). In practice, we find that using a nearest-neighbor distance estimator, e.g., the $N = 2$nd-nearest neighbor with $D_2 < 0.25$ Mpc, identified the majority of galaxies with $\mathcal{P}_z > 0.4$ within $R_{\rm proj} \lesssim 1$ Mpc of the cluster. However, *all* of the D_N estimators selected only a small fraction ($\lesssim$20%) of quiescent galaxies with $\mathcal{P}_z > 0.4$ within 1 Mpc $< R < 1.5$ Mpc from the cluster: the *N*th nearest neighbor distances of these galaxies are simply too large to place them in high local number density regions based on this statistic. Haas et al. (2011) showed that including a requirement on the stellar-mass ratio between neighboring galaxies in the density estimator improves the strength of the correlation between halo mass and density. However, our tests showed that this offers no improvement. Indeed, by requiring neighboring galaxies to be at least as massive as the galaxy in question, nearly all of the most massive galaxies in the cluster are shifted to "low" density regions because there are *no* other galaxies of comparable mass in the sample (and therefore the distance to the *N*th nearest neighbor with comparable mass becomes very large).

It has been shown that *N*th nearest neighbor measurements are good probes of internal cluster properties and galaxy-group-sized halos while fixed aperture methods better examine the cluster as a whole (Muldrew et al. 2012). For this reason, Woo et al. (2012) conclude that using the relative projected distance of a satellite from its halo center is better suited to studying processes associated with clustering on the largest scales than *N*th-nearest neighbor statistics. Moreover, we are motivated by the results from other studies that have found that the environment affects galaxies as they become satellites of larger dark-matter halos, whereas the evolution of central galaxies depends primarily on the halo mass (see Section 1). Therefore, here we adopt the projected distance from the cluster center as our measure of environment for our study. We define our samples as the "cluster" (with $R_{\rm proj} < 1.5$ Mpc) and "field" (with $R_{\rm proj} > 3$ Mpc). In addition, we will divide the "cluster" sample spatially into two subsamples: the cluster center with $R_{\rm proj} < 1.0$ Mpc and the cluster outskirts defined as the annulus with 1.0 Mpc $< R_{\rm proj} < 1.5$ Mpc.

4. THE RELATION BETWEEN ENVIRONMENT, MORPHOLOGY, COLOR, AND MASS AT $z = 1.6$

Figure 1 shows the relation between the $U-B$ rest-frame color and stellar mass for galaxies in our sample in the cluster ($R_{\rm proj} < 1.5$ Mpc) and the field ($R_{\rm proj} > 3$ Mpc), divided into subsamples of disk-dominated galaxies (Sérsic index $n < 2$) and bulge-dominated galaxies (Sérsic index $n > 2$).

In all panels, a strong $U-B$ color–mass and color–mass–morphology relation is apparent. Galaxies with high stellar mass have red colors (similar to, Williams et al. 2009; Quadri et al. 2012). The Sérsic index is correlated with mass and

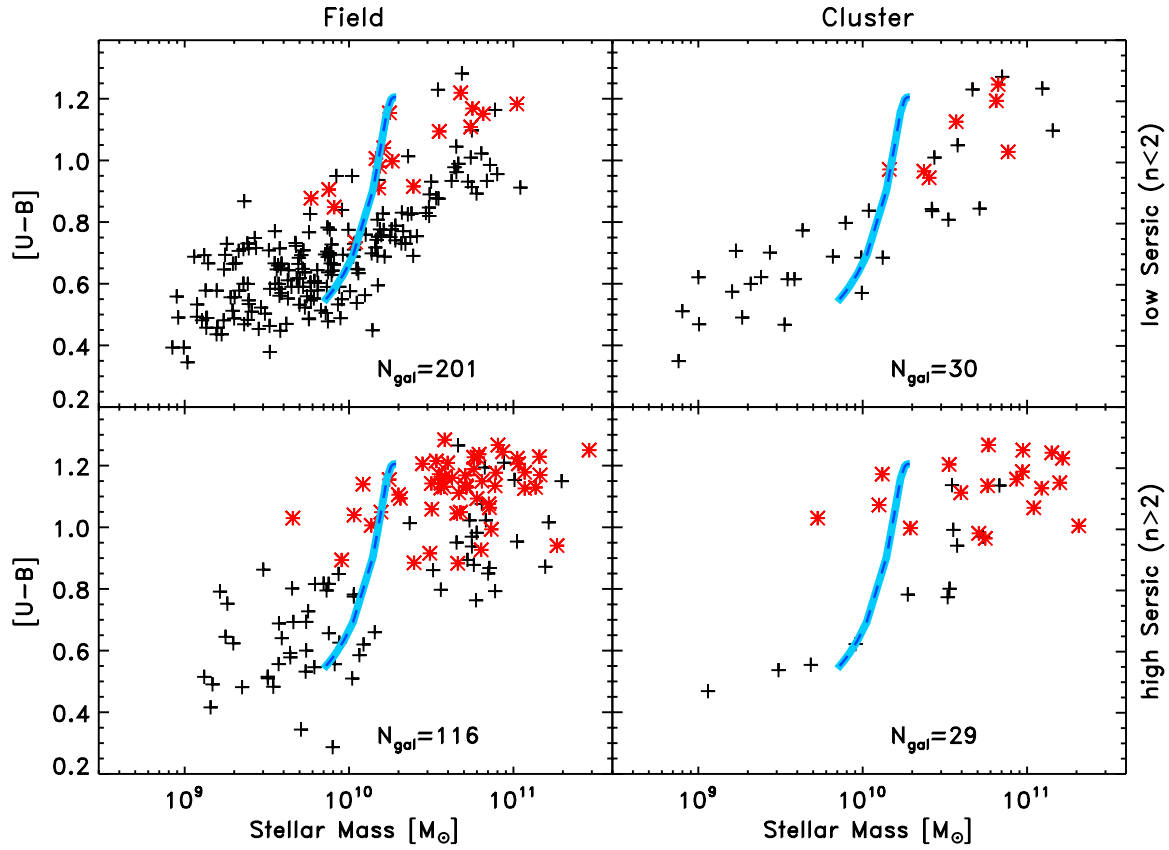

Figure 1. The rest-frame $U-B$ color–stellar mass relation for galaxies at $z = 1.6$. Each panel shows a subset of galaxies in the field and cluster with high and low Sérsic index. The left column shows the relation for galaxies in the field, $R_{\rm proj} > 3$ Mpc from the cluster center. The right column shows the relation for the cluster, with $R_{\rm proj} < 1.5$ Mpc. The upper row shows the relation for the subsample with low Sérsic indices ($n < 2$), and the lower row shows the subsamples with high Sérsic indices ($n > 2$). The red-colored points denote objects that satisfy the color selection for quiescent galaxies. The thick blue lines denote the estimated stellar–mass completeness for stellar population with a maximal mass-to-light ratio, which formed in burst at $z_f = 5$ with solar metallicity and subsequent passive evolution. Our analysis is complete for all galaxies with stellar masses $>2 \times 10^{10}\,M_{\odot}$, where our analysis shows our quantitative morphological parameters are robust.

(A color version of this figure is available in the online journal.)

color. Exactly half (82/164) of bulge-dominated ($n > 2$) galaxies in our sample lie on the red sequence, and the majority (238/269 = 88.5%) of disk-dominated galaxies ($n < 2$) reside in the blue cloud. Disk-dominated galaxies populate the full range of $U-B$ color. This is similar to the findings of previous studies at this redshift, for example, Wuyts et al. (2011) and Bell et al. (2012) and references therein.

Figure 1 also shows the color–mass–morphology distributions for galaxies with colors consistent with older, passively evolving stellar populations. We selected these "quiescent" galaxies using a variant of the *UVJ* selection (Wuyts et al. 2007; Williams et al. 2009) based on the observed $z-J$ and $J-[3.6]$ colors as defined by Papovich et al. (2012),

$$\begin{aligned}(z-J)_{\rm AB} &\geqslant 1.3 \text{ mag}\\ (J-[3.6])_{\rm AB} &\leqslant 2.1 \text{ mag}\\ (z-J)_{\rm AB} &\geqslant 0.5 + 0.55(J-[3.6])_{\rm AB}.\end{aligned} \quad (1)$$

This color-selection classification is efficient in isolating galaxies with very different sSFRs. In Papovich et al. (2012), we showed that when using this color selection, the majority (∼90) of quiescent galaxies selected have sSFRs $< 10^{-2}$ Gyr^{-1}. Therefore, while their SFR may not be zero, it is highly "suppressed" (e.g., Kriek et al. 2006). In contrast, galaxies that do not satisfy our definition for "quiescent" have sSFRs ∼1 Gyr^{-1}, at least one order of magnitude higher, which are characteristic of galaxies on the star-forming "sequence" (e.g., Daddi et al. 2007; Noeske et al. 2007). Therefore, although strictly speaking the color-selection criteria in Equation (1) separates galaxies exhibiting highly suppressed star formation from those that do not, for brevity, we refer to these two samples as "quiescent" and "star-forming" galaxies, respectively.

For much of the analysis here, we use a one-sided Wilcoxon–Mann–Whitney rank-sum (WMW) test (Mann & Whitney 1947) to place a significance on the likelihood that the cluster and field galaxies have similar properties and are drawn from the same parent population. A summary of these likelihoods is given as probabilities (p-values) in Table 1.

4.1. Do the $U-B$ Colors Depend on Environment?

We do observe a slight increase in the $U-B$ color of galaxies associated with the cluster compared to the field. This is illustrated in Figure 2, which shows the cumulative distribution of $U-B$ color for both samples using the data for the CANDELS subset. The WMW test demonstrates that the CANDELS galaxies in the cluster have higher $U-B$ color, with a WMW significance $p = 0.069$. Using the larger full UDS sample improves this significance, with $p = 0.033$ ($\simeq 2\sigma$).

Most of the difference in the $U-B$ colors stems from differences in the colors of the star-forming galaxies. The WMW test for the $U-B$ colors finds no difference in the distributions for the quiescent galaxies ($p \gtrsim 0.3$ for all samples). The

Table 1
Summary of Wilcoxon–Mann–Whitney U Probabilities Comparing the Properties of $z = 1.6$ Cluster and Field Galaxies in the CANDELS UDS Field

Sample	$N_{\rm cluster}$	$N_{\rm field}$	$p(U-B)$	$p(\log M_*)$	$p(\log$ sSFR$)$	$p(r_{\rm eff})$	$p(n)$
(1)	(2)	(3)	(4)	(5)	(6)	(7)	(8)
All galaxies				$\log M_*/M_\odot > 10.30$			
UDS	56	2061	0.0331	0.125	0.296	...	...
CANDELS	37	110	0.0692	0.177	0.218	0.422	0.0800
All galaxies				$10.30 < \log M_*/M_\odot < 10.95$			
UDS	43	1701	0.100	0.308	0.412	...	...
CANDELS	27	94	0.229	0.390	0.263	0.493	0.091
Quiescent galaxies				$\log M_*/M_\odot > 10.30$			
UDS	35	1083	0.458	0.0781	0.216	...	...
CANDELS	21	51	0.397	0.0646	0.202	0.0571	0.0234
Quiescent galaxies				$10.30 < \log M_*/M_\odot < 10.95$			
UDS	24	870	0.291	0.365	0.292	...	...
CANDELS	13	41	0.292	0.310	0.420	0.107	0.0164
Star-forming galaxies				$\log M_*/M_\odot > 10.30$			
UDS	21	978	0.0699	0.466	0.409	...	...
CANDELS	16	59	0.0737	0.339	0.193	0.280	0.238
Star-forming galaxies				$10.30 < \log M_*/M_\odot < 10.95$			
UDS	19	831	0.0586	0.353	0.444	...	...
CANDELS	14	53	0.137	0.254	0.297	0.181	0.457

Notes. (1) Description of samples used, (2) number of cluster galaxies in WMW test, (3) number of field galaxies used in WMW test. Other columns are the WMW significance of the difference in the cluster and field samples between the distributions of (4) stellar-mass, (5) specific SFR, (6) effective radii, (7) Sérsic indices. Low probabilities (p-value) indicate more significant differences in the distributions.

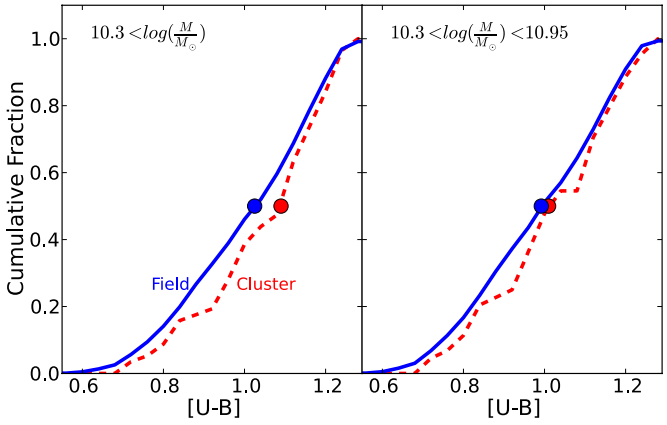

Figure 2. The cumulative distribution of rest-frame $U-B$ colors for all galaxies in the field ($R_{\rm proj} > 3$ Mpc, solid blue line) and in the cluster ($R_{\rm proj} < 1.5$ Mpc, dashed red line). Each curve is normalized to the total number of galaxies in that sample (these curves include all galaxies in the UDS, not only those in the CANDELS field). The left panel shows the distribution for all quiescent galaxies with stellar masses $>2\times10^{10}\ M_\odot$. The circle points on each curve show the median value of the distributions. There is weak evidence that the galaxies associated with the cluster have a median $U-B$ color that is $\Delta(U-B) \sim 0.1$ mag redder than those in the field. The WMW gives $p = 0.033$ for the total UDS samples, but declines to $p = 0.069$ using only the CANDELS samples. The right panel shows a subset with moderate stellar mass 2×10^{10}–$9\times10^{10}\ M_\odot$. The WMW test finds a reduced significance, $p > 0.100$ (see Table 1).

(A color version of this figure is available in the online journal.)

star-forming galaxies in contrast show slight evidence that the $U-B$ colors of the galaxies in the cluster are redder, although the significance is weak with $p = 0.07$ (about 1.5σ). There is little difference in this p-value for the comparison between the smaller CANDELS samples and the larger UDS samples.

If this difference in the $U-B$ colors of the star-forming galaxies is real, then it would provide evidence that the star-forming galaxies associated with the cluster have more dust extinction, which reddens the colors. This could imply that the SFRs we derive from the SED fitting may be lower limits, missing highly extincted star formation, which is indicated by the redder $U-B$ colors.

For reasons discussed below, we tested if galaxies at larger clustercentric distances, defined by the annulus 1 Mpc $< R_{\rm proj} <$ 1.5 Mpc, have different $U-B$ colors compared to those galaxies within $R_{\rm proj} < 1$ Mpc from the cluster. However, the WMW test gives no measurable difference with p-values > 0.11 for all subsamples, which is not significant. Therefore, the cluster galaxies within $R_{\rm proj} < 1$ Mpc have similar $U-B$ colors as those galaxies within 1 Mpc $< R_{\rm proj} <$1.5 Mpc. We repeated this test for only the subsample of galaxies with $M = (2$–$9)\times10^{10}\ M_\odot$, but find no substantial differences.

4.2. Do the Specific SFRs of Galaxies Depend on Environment?

Considering the combined samples (quiescent and star-forming galaxies), the WMW does not rule out the hypothesis that the sSFR distributions are drawn from the same parent populations (all have $p > 0.22$), and we see no difference in the sSFR distributions for more restrictive samples of quiescent or star-forming galaxies. We also see no significant difference using either the smaller CANDELS sample or larger UDS sample. There is no apparent difference in the sSFR distributions between the cluster and the field, nor is there any significant difference in the distributions for galaxies in the cluster core ($R_{\rm proj} < 1$ Mpc) and those in the $R_{\rm proj} = 1$–1.5 Mpc annulus.

On the surface, this result appears to contrast some studies that find an increase in the SFR (or SFR surface density) of galaxies in the cores of clusters at this redshift (e.g., Tran et al. 2010; Kocevski et al. 2011). For example, Tran et al. (2010) found an elevated IR luminosity projected surface density associated with this cluster compared to the field. We attribute this apparent discrepancy to the fact that in our study, we have not included IR data, and therefore our SFRs (and sSFRs) may be underestimated. Indeed, this is consistent with the star-forming galaxies in the cluster having redder $U-B$ rest

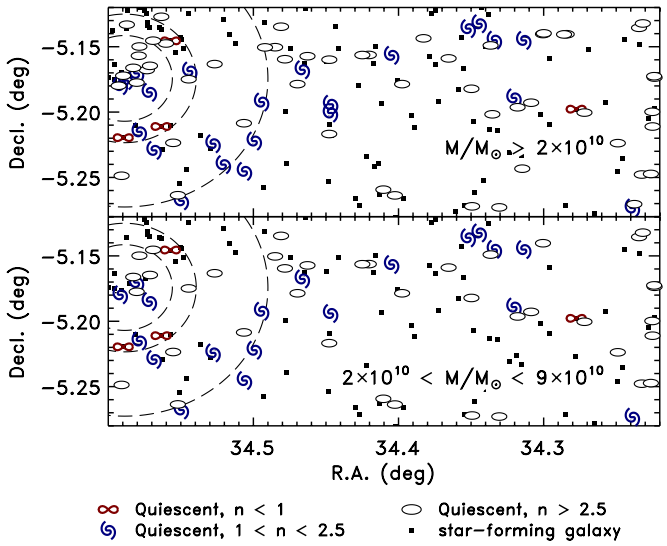

Figure 3. The spatial distribution of galaxies at $z = 1.6$ in the CANDELS UDS field. The symbols denote quiescent (large symbols) and star-forming galaxies (small boxes), as labeled. For the quiescent galaxies, the symbol type corresponds to Sérsic index, as indicated in plot legend. The concentric dashed circles show projected distances of $R_{\rm proj} = 1$, 1.5, and 3 Mpc from the astrometric center of the cluster using the coordinates of Papovich et al. (2010). The quiescent galaxies in the annulus 1 Mpc $< R_{\rm proj} <$ 1.5 Mpc have lower Sérsic indices and larger effective sizes compared to other quiescent galaxies.

(A color version of this figure is available in the online journal.)

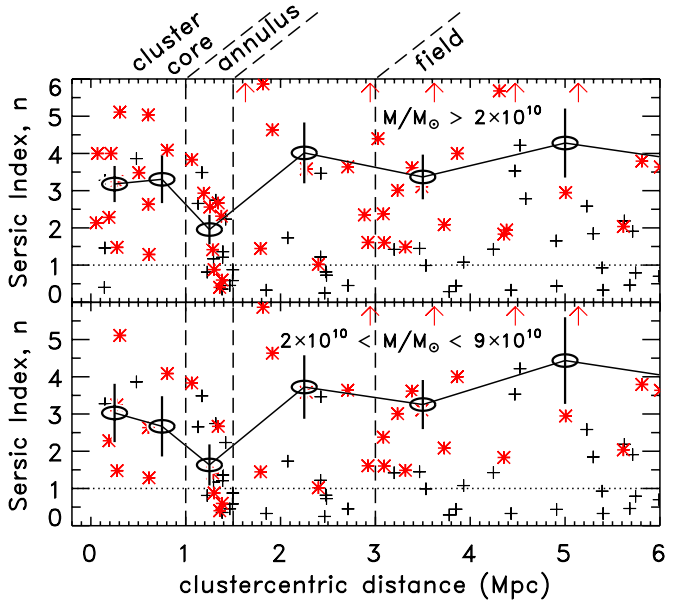

Figure 4. The Sérsic indices of galaxies in the CANDELS imaging are plotted vs. their clustercentric distances. The red stars and black crosses represent galaxies classified as "quiescent" and "star-forming" respectively using a rest frame *UVJ* color selection described in Section 4. The open ovals are median values for only the quiescent galaxies with vertical bars depicting the interquartile range. The dashed vertical lines indicate the locations of the cluster core, the 1–1.5 Mpc annulus, and the field. All galaxies above our stellar mass limit are plotted in the top panel while only intermediate mass galaxies are plotted on the bottom. This plot nicely illustrates the drop in Sérsic indices for quiescent galaxies located within the 1–1.5 Mpc annulus around the cluster core. It can also be seen that only in this region do we find quiescent galaxies with Sérsic indices less than 1 (shown as the horizontal dotted line).

(A color version of this figure is available in the online journal.)

frame colors from Section 4.1. As discussed above, this may imply these galaxies have high extinction, which would imply higher extinction-corrected SFRs that we are missing in our measurements.

4.3. Do the Stellar Masses Depend on Environment?

In general, there is no substantial difference in the distribution of stellar masses when all galaxies (quiescent and star-forming) are considered in the field and the cluster. For the more restrictive sample of quiescent galaxies only, those associated with the cluster show a possible increase in stellar mass relative to the field. The WMW test gives a significance $p = 0.065$ for the CANDELS samples. However, this increases to $p = 0.078$ when all galaxies in the larger UDS samples are considered, implying a weaker significance. Therefore, there is slight evidence (1.5σ significance) that quiescent galaxies associated with the cluster have larger stellar masses compared to those in the field. The difference appears to be driven by the higher stellar masses of the quiescent galaxies in the cluster compared to the field, which is evident in Figure 1.

The stellar masses of galaxies in the 1 Mpc $< R_{\rm proj} <$ 1.5 Mpc annulus show evidence of being different from those with $R_{\rm proj} <$ 1 Mpc. Considering all galaxies (star-forming and quiescent), the galaxies within $R_{\rm proj} <$ 1 Mpc have stellar masses approximately a factor of 1.9 higher than those within 1 Mpc $< R_{\rm proj} <$ 1.5 Mpc (with WMW $p = 0.0053$). This significance is reduced ($p = 0.078$) when considering only quiescent galaxies. Interestingly, there is no difference between the galaxies within 1 Mpc $< R_{\rm proj} <$ 1.5 Mpc and those in the field, $R_{\rm proj} > 3$ Mpc, ($p > 0.2$), suggesting that galaxies in this annulus share a mass distribution more characteristic of the field at this redshift than the highest-density region associated with the cluster. This is possible evidence that these galaxies were recently members of the field and are in the process of being accreted into the cluster environment.

4.4. Do the Sérsic Indices of Galaxies Depend on Environment?

We now compare the difference in Sérsic indices between the cluster and field populations in more detail. This is illustrated in Figures 3 and 4. Figure 3 shows the astrometric positions of quiescent and star-forming galaxies at $z = 1.6$ in the CANDELS field. The symbols correspond to the Sérsic index of the quiescent galaxies. Figure 4 shows the Sérsic indices of galaxies in the CANDELS field as a function of their clustercentric distance. These figures show that there appears to be an excess of galaxies with $n < 2.5$ in the annulus 1 Mpc $< R_{\rm proj} <$ 1.5 Mpc from the cluster relative to either the sample with $R_{\rm proj} <$ 1 Mpc or the field sample ($R_{\rm proj} > 3$ Mpc), and that this effect is driven by intermediate mass galaxies. It is also apparent that quiescent galaxies with $n < 1$ are only found in the 1 Mpc $< R_{\rm proj} <$ 1.5 Mpc annulus. As discussed in Section 3.1, to test if this is a result of our choice of F125W bandpass or analysis, we checked our Sérsic indices against those computed independently from the F160W data from Bell et al. (2012), and we found no change.

4.4.1. Comparison between the Cluster and the Field

Table 1 shows the WMW p-values comparing the properties of galaxies in the cluster and field environments. Based on our analysis, there is no evidence that star-forming galaxies in the field and cluster have differences in their Sérsic indices.

We do observe differences in the distributions of Sérsic indices for quiescent galaxies. There is an envelope in the Sérsic index and stellar mass distribution for quiescent galaxies: more

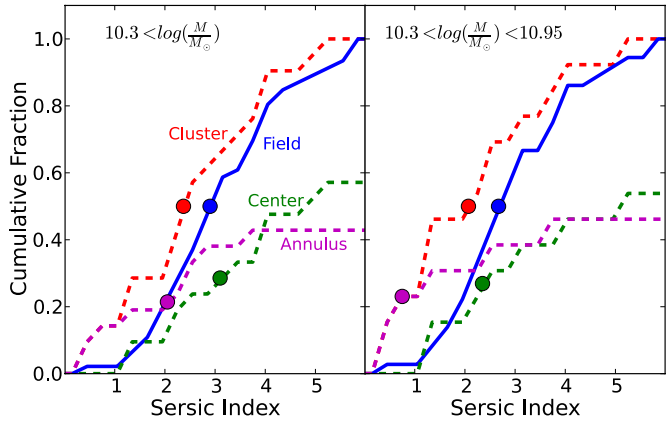

Figure 5. The cumulative Sérsic-index distribution for quiescent galaxies in the field (solid blue line) and in the cluster (dashed red line). The curves for the total cluster and total field samples are normalized to the number of galaxies in each sample. The curves for the cluster subsamples ("field" and "annulus") are normalized by the number of galaxies in the total cluster sample. The left panel shows the distribution for all quiescent galaxies with stellar masses $>2 \times 10^{10}\,M_{\odot}$. The left panel shows a subset with moderate stellar mass 2×10^{10}–$9 \times 10^{10}\,M_{\odot}$. The circular points on each curve show the median value of the distributions. The quiescent galaxies associated with the cluster have smaller median Sérsic indices, and this is most pronounced in the moderate-mass subsample. The green (purple) dashed curve shows the contributions to the cluster cumulative distribution from quiescent cluster galaxies in the cluster "center" with $R < 1$ Mpc ("annulus" with 1 Mpc $< R <$ 1.5 Mpc). In both panels, the lower Sérsic indices of quiescent cluster galaxies is driven by the quiescent galaxies associated with the cluster in an annulus 1 Mpc $< R <$ 1.5 Mpc, which have the lower median values.

(A color version of this figure is available in the online journal.)

massive quiescent galaxies generally have higher Sérsic indices, and only a few of the most massive ($> 9 \times 10^{10}\,M_{\odot}$) galaxies have $n < 2$ (Figure 1). Most, $81/108 = 75\%$, of the quiescent galaxies in both the field and cluster have high Sérsic indices, $n > 2$, and are bulge-dominated (consistent with Bell et al. 2012; Wuyts et al. 2011; Papovich et al. 2012). However, more notably, the fraction of galaxies with *low* Sérsic index $n < 2$ that are quiescent is significantly higher in the cluster ($6/16 = 38\%$) compared to the field ($8/43 = 15\%$), for galaxies above our mass limit. This is significant at about 2.5σ from binomial statistics, although it is based on small numbers of galaxies. As illustrated in Figures 3 and 4 and as we discuss below, most of this difference comes from galaxies in the annulus 1 Mpc $< R_{\rm proj} <$ 1.5 Mpc from the cluster, and suggests some mechanism suppresses star formation in galaxies with low Sérsic index at large clustercentric radii.

The WMW probabilities in Table 1 show the evidence for differences in the Sérsic indices of galaxies associated with the cluster and the field. Most of this difference is isolated to the quiescent galaxies: star-forming galaxies in both the field and cluster have median Sérsic indices $n_{\rm med} \simeq 1.4$, with no significant differences, $p > 0.2$. Quiescent galaxies associated with the cluster have lower median Sérsic indices, $n_{\rm med} = 2.6$ versus $n_{\rm med} = 3.3$ in the field, and the WMW test shows this is significant with $p = 0.023$ (approx. 2σ) considering the full sample with $M > 2 \times 10^{10}\,M_{\odot}$. Figure 5 shows the cumulative distribution of the Sérsic indices of quiescent galaxies in the field and the cluster.

The right panel of Figure 3 shows the cumulative distributions for the more restrictive subsamples of quiescent galaxies with moderate stellar mass, 2×10^{10}–$9 \times 10^{10}\,M_{\odot}$. Here the median Sérsic index is $n_{\rm med} = 2.4$ for the cluster galaxies and $n_{\rm med} =$ 2.8 for the field galaxies, and the significance increases to $p = 0.016$.

This result has a significance of $\approx 2\sigma$, and is based on relatively small samples: 21 quiescent galaxies with stellar mass $>2 \times 10^{10}\,M_{\odot}$ that lie within $R_{\rm proj} < 1.5$ Mpc from the cluster as covered by CANDELS (Table 1). To test further the significance of this result, we used a bootstrap Monte Carlo test to estimate a likelihood that we obtained the observed difference in Sérsic indices by chance. We used as a parent sample the combined samples of all quiescent galaxies in the cluster and field. We then constructed 10,000 pairs of cluster-sized and field-sized samples of N(cluster) and N(field) objects randomly selecting from the parent sample (with replacement), where N(cluster) and N(field) are equal to the size of the original cluster and field samples, respectively. We then recomputed the WMW p value between each pair of random cluster and field samples. In this test, we obtained a p value as small (or smaller) as the one we observe in only 0.6% of the random samples when drawing from the full sample of galaxies with $M > 2 \times 10^{10}\,M_{\odot}$ (this increases slightly to 0.9% of cases for $M = 2 \times 10^{10}$–$9 \times 10^{10}\,M_{\odot}$ moderate-mass samples). Therefore, the likelihood that we would have obtained our result by chance if there were no actual difference between the cluster and field objects is smaller than 1% (equivalent to the probability of $>2.6\sigma$ significance for a Gaussian distribution).

4.4.2. Comparison between the Cluster Core and the 1 Mpc $< R_{proj} <$ 1.5 Mpc Annulus

As shown in Figure 5, the quiescent galaxies in the 1 Mpc $< R_{\rm proj} <$ 1.5 annulus have lower median Sérsic indices $n_{\rm med}^{\rm 1-1.5\,Mpc} = 2.1$, compared to those within 1 Mpc of the center of the cluster, which have median $n_{\rm med}^{\rm <1\,Mpc} = 3.0$. Indeed, four out of the six moderate-mass quiescent galaxies in the annulus have Sérsic indices $n < 2.5$, including three galaxies with $n < 1$. This is evident in Figures 3 and 4, which show that these low-Sérsic-index quiescent galaxies are found preferentially at 1–1.5 Mpc from the cluster. This difference is even more apparent considering the most restrictive moderate-mass subsample with 2×10^{10}–$9 \times 10^{10}\,M_{\odot}$. For this sample, the median Sérsic indices are $n = 1.0$ and $n = 2.4$ for the annulus and cluster core, respectively.

The significance of this result is somewhat limited by the small number of objects in the samples: there are only 95 quiescent galaxies in our cluster and field samples combined. To measure the significance of this result, we considered two Monte Carlo bootstrap simulations to determine how often we would obtain this result by chance.

We first calculate how often we would obtain the results by chance if the quiescent galaxies in the 1–1.5 Mpc annulus are randomly drawn from the parent field sample. For this test we constructed two random samples, one having N(1–1.5 Mpc) members (the number of quiescent galaxies in the 1–1.5 Mpc annulus) and the other having N(field) members. Both samples are drawn from the quiescent field population with replacement. From this bootstrap test, we found that the WMW p value was smaller than the measured value in only 0.44% of the cases, which corresponds to a significance of $\approx 2.6\sigma$ (assuming a Gaussian distribution). Therefore, it seems that even with the small sample sizes here, the lower Sérsic indices of the quiescent galaxies in the annulus 1 Mpc $< R_{\rm proj} <$ 1.5 Mpc are statistically significant compared to quiescent galaxies in the field.

We next repeated this bootstrap test to estimate how often we would obtain the results by chance if the quiescent galaxies in the annulus are randomly drawn from the parent cluster quiescent sample. Again, we constructed random samples, one having N(1–1.5 Mpc) members and one having N(<1 Mpc) members. Here, we find that the likelihood that the quiescent galaxies in this annulus are drawn from the same population as those in the rest of the cluster is $p_{\rm bootstrap} = 0.039$ ($\approx 1.8\sigma$) primarily because of the smaller number of quiescent galaxies in the cluster sample. Larger samples of quiescent galaxies (especially those in clusters) at this redshift are required to improve the statistical significance of this observation.

To summarize this section, there is evidence that the quiescent galaxies in the cluster have lower average Sérsic indices compared to quiescent galaxies in the field. Furthermore, there is evidence that this result is driven by a population of quiescent galaxies in an annulus 1–1.5 Mpc from the cluster. Members of this population are found to have Sérsic indices inconsistent with random samples of quiescent galaxies taken from the cluster core ($R_{\rm proj} < 1$ Mpc) or from the field. Instead, they are morphologically more similar to star-forming galaxies found in all environments.

4.5. Do the Effective Radii of Galaxies Depend on Environment?

Because the quiescent galaxies in the cluster show evidence for smaller Sérsic indices, we also compared the effective radii of these galaxies to those in the field. The median effective radius of quiescent galaxies with stellar mass $>2 \times 10^{10}\,M_{\odot}$ associated with the cluster is $r_{\rm eff,med}^{\rm cluster} = 2.0$ kpc compared to those in the field which have $r_{\rm eff,med}^{\rm field} = 1.4$ kpc. (We remind the reader that these radii are the circularized effective radius.) The WMW test gives a probability $p = 0.057$. This is nearly identical to the findings of Papovich et al. (2012), who used the same data but with slightly different selection criteria and mass limits to focus on the quiescent galaxies (see also Section 2). Figure 6 shows the cumulative distribution of the effective radii of quiescent galaxies in the field and cluster, which illustrates that the cluster galaxy sizes are larger on average.

We also considered the effective sizes of the quiescent galaxies within $R_{\rm proj} < 1$ Mpc of the cluster center compared to those in the annulus 1 Mpc $< R_{\rm proj} <$ 1.5 Mpc because these show evidence for having different Sérsic indices. Figure 6 shows the cumulative distributions of these subsamples. The quiescent galaxies in the 1 Mpc $< R_{\rm proj} <$ 1.5 Mpc annulus have median effective radii, $r_{\rm eff,med}^{\rm 1-1.5\,Mpc} = 2.7$ kpc, about 1.3 times larger than other quiescent galaxies in the cluster or the field.

Because of the relatively small size of our galaxy samples, we again used a Monte Carlo bootstrap simulation (similar to the previously described simulations) to test the significance of these results. Based on this test, the likelihood that the quiescent galaxies in this annulus are drawn from the cluster sample is 9.6%. Similarly, the likelihood that the quiescent galaxies in this annulus are drawn from the same population as those in the field is 8.3%. Given the relatively small sample size, it seems that larger samples would be able to further test these trends.

The results of this section can be summarized as follows: we find that quiescent galaxies associated with the cluster have low Sérsic indices and possibly larger effective radii (when compared with quiescent galaxies in the field) consistent with disk-like morphologies ($n \sim 1$). This effect is driven by galaxies located in an annulus 1–1.5 Mpc from the center of the cluster,

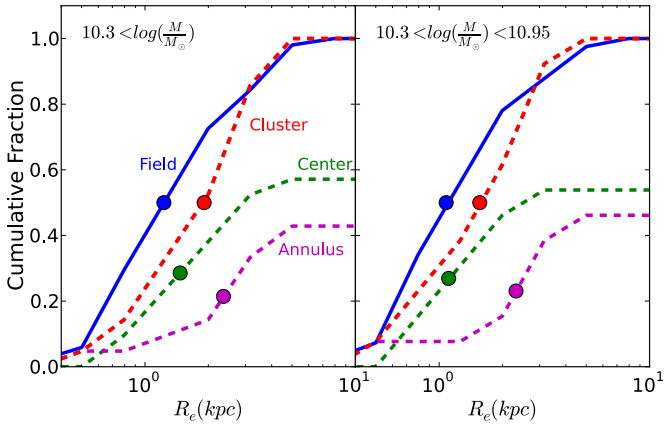

Figure 6. The cumulative distribution of effective radii for quiescent galaxies in the field ($R_{\rm proj} > 3$ Mpc, solid blue line) and in the cluster ($R_{\rm proj} < 1.5$ Mpc, dashed red line). Each curve is normalized to the total number of galaxies in each sample. The left panel shows the distribution for all quiescent galaxies with stellar masses $>2 \times 10^{10}\,M_{\odot}$. The right panel shows a subset with moderate stellar mass 2×10^{10}–$9 \times 10^{10}\,M_{\odot}$. The quiescent galaxies associated with the cluster generally have larger median effective radii. In each panel, the green (purple) dashed curve shows the contribution to the cluster cumulative distribution from quiescent galaxies in the cluster "center" with $R < 1$ Mpc ("annulus" with 1 Mpc $< R <$ 1.5 Mpc). The circle points show the median value for each distribution. Quiescent galaxies associated with the cluster in an annulus 1 Mpc $< R <$ 1.5 Mpc have larger median effective radii by factors of two compared to the field.

(A color version of this figure is available in the online journal.)

whereas quiescent galaxies in the cluster core and field exhibit Sérsic indices more typical of a bulge dominated morphology. Furthermore, the most massive galaxies are located in the cluster core while stellar masses of galaxies in the annulus are comparable to those found in the field. This suggests that the sample of quiescent galaxies found 1–1.5 Mpc from the center of the cluster is "contaminated" with recently quenched star-forming galaxies accreted from the field.

5. DISCUSSION

5.1. The Relation between Color, Stellar Mass, and Morphology in the Cluster and Field at $z = 1.6$

We study how the relationship between galaxy color, stellar mass, and morphology depend on galaxy environment by examining these relations in the field and in a forming cluster at $z \sim 1.6$. We find evidence of a possible correlation between galaxy density with color and mass for galaxies with stellar masses $>2 \times 10^{10}\,M_{\odot}$: compared to galaxies in the field, the cluster galaxies (with $R_{\rm proj} < 1.5$ Mpc) have redder rest frame $U-B$ colors and higher stellar masses. The color difference appears driven by star-forming galaxies (we find no difference in the rest-frame $U-B$ colors of quiescent galaxies). We interpret this as evidence for increased dust-obscured star formation in galaxies closer to the cluster, supported by the higher IR-luminosity density in these galaxies found by Tran et al. (2010). The stellar mass difference appears driven by the more massive quiescent galaxies with $>9 \times 10^{10}\,M_{\odot}$(see Section 4.2 and Figure 4), and we interpret this as evidence that the most massive galaxies at this redshift in this field are associated with the cluster.

There are morphological differences in the quiescent galaxy populations associated with the cluster and the field. Combining our observations with the results from our previous study (Papovich et al. 2012), we find two main differences between

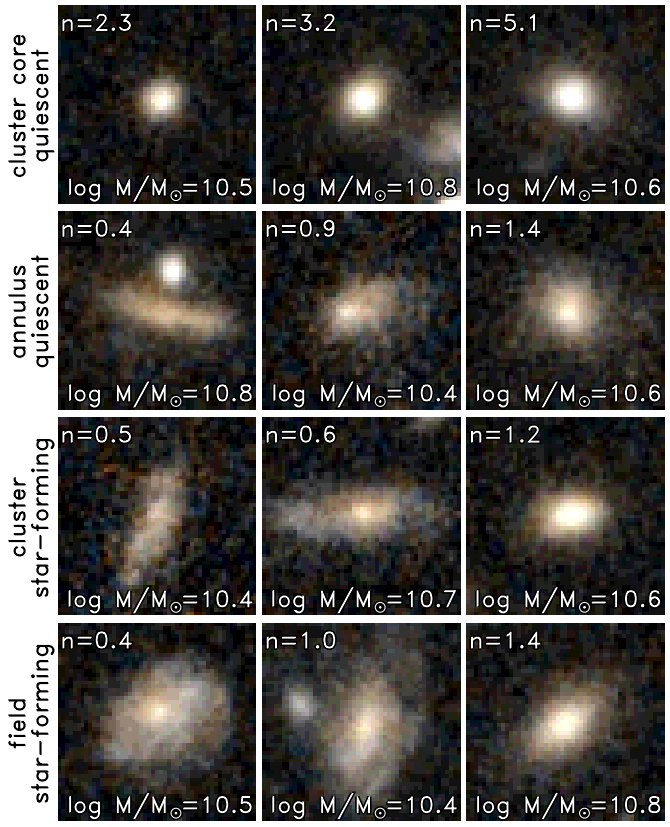

Figure 7. Examples of quiescent galaxies in the annulus 1 Mpc $< R_{\rm proj} <$ 1.5 Mpc and low Sérsic index ($n < 2$) and other galaxy subsamples. Each panel spans 12″ on a side (about 100 kpc at $z = 1.6$), and the colors show the *HST* F125W, (F125W+F160W)/2, and F160W as blue, green, and red, respectively. These images illustrate that these quiescent galaxies have similar morphologies as star-forming galaxies in both the cluster and field selected with low Sérsic indices and over a similar range of stellar mass. The top row shows quiescent galaxies in the core with similar stellar masses but more typical, higher Sérsic indices.

(A color version of this figure is available in the online journal.)

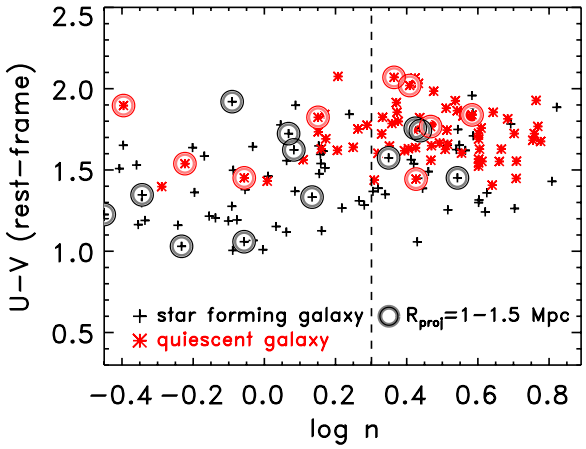

Figure 8. The Sérsic indices, n, vs. the rest-frame $U - V$ color for galaxies with stellar mass $>2 \times 10^{10}\ M_{\odot}$. Bell et al. (2012) have argued that Sérsic index best correlates with increasing $U - V$ color. We reproduce that result here, as most quiescent galaxies lie above $n > 2$, indicated by the dashed line. Quiescent and star-forming galaxies in the subsample with 1 Mpc $< R <$ 1.5 Mpc of the cluster center are indicated with large circles. A high fraction (≈50%) of the quiescent galaxies in this annulus have $n < 2$, compared to <15% of quiescent galaxies overall.

(A color version of this figure is available in the online journal.)

the morphologies of quiescent galaxies in the field and that of the cluster. First, Papovich et al. (2012) found a lack of "compact" quiescent galaxies with $r_{\rm eff} \sim 1$ kpc in the cluster while such objects are present in the field. Similarly, many of these quiescent galaxies in the cluster show evidence for extended disks. Our analysis here reproduces the findings of Papovich et al. (2012), and here we report evidence that the Sérsic indices of the quiescent galaxies in the cluster are lower than for such galaxies in the field.

5.2. The Nature of Quiescent Galaxies in the Annulus $R_{proj} = 1$–1.5 Mpc

The population of quiescent galaxies in the annulus defined by projected distances 1 Mpc $< R_{\rm proj} <$ 1.5 Mpc from the cluster show the most differences in morphology compared to the field. As discussed in Section 4.4, galaxies in this annulus have higher $r_{\rm eff}$ and lower Sérsic indices. Indeed, considering the full subsample with $M > 2 \times 10^9\ M_{\odot}$, their median values are $r_{1-1.5\,\rm Mpc} = 2.7$ kpc and $n_{1-1.5\,\rm Mpc} = 2.1$ (compared to medians $r_{<1\ \rm Mpc} = 1.5$ kpc and $n_{<1\ \rm Mpc} = 3.1$ in the cluster center). The quiescent galaxies in the $R_{\rm proj} = 1$–1.5 Mpc annulus are more typical of star-forming galaxies in the field and cluster. Figure 7 shows examples of these quiescent galaxies in the cluster annulus with low Sérsic index ($n < 2$), and compares these with examples of star-forming galaxies with similar masses and Sérsic indices ($n < 2$). These examples illustrate that the quiescent galaxies have morphologies similar to some star-forming galaxies. In contrast, the figure also shows quiescent galaxies in the cluster core with more typical, higher Sérsic indices ($n > 2$). These have very different morphologies when compared to annulus quiescent galaxies with low Sérsic indices. The star-forming galaxies have an interquartile range of 2.2–4.7 kpc in effective radius and 0.8–3.3 in Sérsic index, consistent with morphologies of these quiescent galaxies in the annulus. Because these galaxies appear morphologically distinct, we speculate about their origin and fate.

Bell et al. (2012) have argued that the Sérsic index correlates the strongest with increasing rest-frame $U - V$ color. We reproduce this relation in Figure 8, which shows the Sérsic index versus $U - V$ color for all $z \sim 1.6$ galaxies in our CANDELS data with stellar mass $>2 \times 10^{10}\ M_{\odot}$.

We find a similar result to that of Bell et al., as most quiescent galaxies lie above $n > 2$. However, many of the quiescent galaxies associated with the 1 Mpc $< R_{\rm proj} <$ 1.5 Mpc annulus appear as outliers. A high fraction (≈50%) of the quiescent galaxies in the annulus 1 Mpc $< R_{\rm proj} <$ 1.5 Mpc have $n < 2$, compared to <15% of quiescent galaxies overall. This leads to differences in the Sérsic index distributions we see for quiescent galaxies in this annulus compared to the other samples (see Section 4.4).

5.3. Environmental Effects on Galaxy Evolution at $z = 1.6$

At $z = 1.6$, there appear to be two evolutionary channels for quiescent galaxies, one that depends on the mass of the galaxy, and another that depends on environment. Mass is likely related to one channel of quiescence because both the field and cluster samples exhibit passive, bulge dominated galaxies ($n > 2$) that show no differences in their sSFRs, or rest-frame $U - B$ colors (see Table 1). This mass-related channel therefore has only a weak dependence on environment (cluster versus field) and is likely driven by processes related to the galaxy halo mass. This is similar to the findings of Peng et al. (2010).

The environment also has some role in the morphological evolution of galaxies. One difference between the cluster and field quiescent galaxies is in their sizes. Cluster galaxies have slightly larger effective radii than quiescent galaxies in the field (see also Papovich et al. 2012) that are significant at $\sim 1.5\sigma$. There are also indications that the cluster galaxies have a higher "dry" merger rate (Lotz et al. 2013), which has been interpreted as evidence that the cluster galaxies have an increased or accelerated evolution. This view is consistent with the evolution of sizes of cluster galaxies, and the cluster luminosity function (Papovich et al. 2012; Rudnick et al. 2012). The higher density region associated with the cluster appears to increase the merger rate of quiescent galaxies over that expected solely in the field. In the case of minor mergers, this has the effect of increasing their radii while only modestly increasing their mass. This process appears to work within $R_{\rm proj} \lesssim$ 1–1.5 Mpc from the cluster center.

The environment also seems to affect quiescent galaxies at higher projected distances from the cluster (1 Mpc $< R_{\rm proj} <$ 1.5 Mpc). It is in this annulus where we see indications that the quiescent galaxies have larger effective radii and lower Sérsic indices (see Section 4.4 and Figure 4). The mass distribution of the quiescent galaxies in this annulus is also different from quiescent galaxies in the cluster center, which suggests that some process affecting galaxies accreted by the cluster is linked to the formation of these galaxies.

As discussed above, the morphologies of the quiescent galaxies in this annulus are more typical of the morphologies of star-forming, disk-dominated galaxies. Interestingly, the projected distances of the galaxies in this annulus lie outside the upper limits of the virial radius estimated from galaxy velocity dispersions ($\simeq$0.9 Mpc, under the assumption the galaxies are fully virialized, Papovich et al. 2010) and analysis of the X-ray data (Pierre et al. 2011, $\simeq$0.5 Mpc). If our findings are confirmed by larger samples to be a general property of cluster galaxies at this epoch, then it is implied that there is a mechanism which induces quiescence at large distances from the cluster center but leaves galaxy morphologies unchanged.

One explanation for these observations is that these disk-dominated quiescent galaxies at projected distances 1 Mpc $< R_{\rm proj} <$ 1.5 Mpc have been preprocessed in smaller group-sized halos, which are now merging with the cluster (e.g., McGee et al. 2009). Figure 3 shows that the late-type quiescent galaxies may be located in $\sim$2 groupings. Moreover, qualitatively, many of the $1 < n < 2.5$ quiescent galaxies in the *field* are not randomly distributed, but rather exist in small groups that are identified using *N*th nearest neighbor measures.[15]

[15] Characterizing overdensity in our sample using the *N*th nearest-neighbor method, we measured no appreciable differences in galaxy properties, using either the $z = 1.6$ sample defined by $\mathcal{P}_z > 0.4$ or the sample selected using the best-fit photometric redshifts in the range $1.5 < z < 1.75$. This may be due to the fact that our samples rely largely on photometric redshifts, which is necessary to be complete for red galaxies at $z \sim 1.6$. Samples based on photometric redshifts will suffer from projection effects along the line of sight (even the "good" photometric redshifts of our data, $\Delta z/(1+z) = 0.04$, yield line-of-sight proper distance uncertainties of 27 Mpc). This will smear any real correlations between galaxy density (environment) and galaxy properties. This is mitigated in lower redshift samples based on spectroscopic redshifts (e.g., Kauffmann et al. 2004; van der Wel et al. 2008; Peng et al. 2010; Cooper et al. 2011). We speculate that the reason we are able to detect differences in the galaxy properties comparing the cluster to the field is that the overdensity of the cluster overcomes the smearing along the line-of-sight from photometric redshifts. Nevertheless, this smearing will affect our results, reducing any intrinsic trends between galaxy properties and environment. Therefore, it also follows that the results here show the *minimum* effect at $z = 1.6$ of environment on galaxy properties such as color, masses, SFRs, specific SFRs, sizes, and Sérsic index.

However, the idea of preprocessing does not explain why the morphological properties of the quiescent galaxies at 1 Mpc $< R_{\rm proj} <$ 1.5 Mpc would be significantly different from quiescent field galaxies. We favor an explanation where quiescent galaxies at projected distances of 1 Mpc $< R_{\rm proj} <$ 1.5 Mpc began as star-forming, disk-dominated galaxies before they entered the proximity of the forming galaxy cluster. At these distances, they undergo truncation of their star formation without disrupting their morphological profiles or sizes. At later times, they will enter the cluster "halo," and because they are quiescent, likely will undergo dissipationless mergers with other quiescent galaxies. This will then reconfigure their morphologies, consistent with the enhanced merger rate of Lotz et al. (2013). The mechanism for this transition from star-forming disk galaxy to quiescent galaxy appears to begin outside the cluster virial radius. If this occurs in galaxy groups, then it affects the galaxies only as they approach the region of the cluster.

This interpretation may be explained by the expectation from theory that as gas falls into the region of large halos, it is shocked to the virial temperature of the halo (e.g., White & Rees 1978; Birnboim & Dekel 2003). Recent cosmological *N*-body and hydrodynamical simulations show that the velocity shock from the virialized region extends beyond the virial radius (Cuesta et al. 2008; Birnboim et al. 2007; Dekel et al. 2009), and this affects both the baryonic gas fraction and the velocities and temperatures of the "shocked" infalling gas out to 1.5–2$R_{\rm vir}$, as well as the stripping of subhalos at 3–4$R_{\rm vir}$. (Kravtsov et al. 2005; Bahe et al. 2012; Behroozi et al. 2013; E. Zinger et al., in preparation).

The quiescent disk-dominated galaxies we observe at 1–1.5 Mpc from the cluster may be inside this hot (shocked) medium, where gas accretion to them is then shut off (Dekel & Birnboim 2006; Croton et al. 2006). This process is often referred to as gas "strangulation" (Balogh et al. 2000). It is possible these galaxies are on their first infall into the cluster: the cluster-crossing time is 5 Gyr (assuming the 1 Mpc radius and typical peculiar velocity of $\approx$400 km s^{-1}, Pierre et al. 2012), and this exceeds the age of the universe at $z = 1.6$. Under the assumption that the galaxies are on their first pass through the cluster (and have not already passed through), effects from a virial-shock-like process seem to be favored because the galaxies lie outside the central cluster region. Other processes that could affect these galaxies such as ram-pressure stripping (Gunn & Gott 1972; Abadi et al. 1999), tidal stripping (Read et al. 2006), and galaxy harassment (Moore et al. 1996) are expected to be more significant nearer the central cluster regions where the galaxy and gas densities are higher. Because it is less likely that the quiescent disk-dominated galaxies at 1–1.5 Mpc have had sufficient time to pass through the cluster, it seems more likely that they have consumed their gas supply and gas accretion has been "strangulated" by the hot medium.

We also cannot rule out the possibility, however, that these galaxies *have* already passed through the outskirts of the larger dark matter potential and are now located at the turn-around radius of the cluster. By passing through the central halo at large radii, the baryonic content of this population could have been altered without significantly restructuring their morphologies. Although we estimate that the crossing times for this cluster may be longer than the age of the universe at this redshift, this structure has grown since earlier epochs, and as it does not yet appear virialized the interpretation of the kinematics is unclear.

Another mechanism that may explain this processing of galaxies at large clustercentric distances is the assembly bias

of dark matter halos (Gao et al. 2005; Wechsler et al. 2006; Croton et al. 2007). Simulations show that halos with early formation redshifts are more strongly clustered than halos of comparable mass that form later. Assembly bias in the nearby universe ($0.01 < z < 0.3$) has been studied in the Sloan Digital Sky Survey by Cooper et al. (2010), who find that galaxies with older stellar populations and higher stellar metallicities are preferentially found in higher density environments. This suggests that at a given mass, early type galaxies in dense environments were formed earlier, and thus ceased forming stars at an earlier epoch. This idea is supported by the comparison of ages of low redshift early-type galaxies between low and high local number density regions. Massive galaxies in high local number density regions appear to form their stellar populations in the range between $z \sim 2$ and $z \sim 5$, while their low local number density counterparts are 1–2 Gyr younger (Thomas et al. 2005).

Simulations show that a cause for this assembly bias is that group-sized halos must compete for mass (both baryonic and dark matter) when in close proximity to much larger dark matter halos. In effect, the group halos will be starved of dark matter and the galaxies they contain will be similarly starved of baryonic gas. These galaxies will exhaust their supply of star-forming gas more quickly than galaxies located in similar halos in isolation. As this starvation is not directly associated with mergers or other more direct galaxy interactions, it is likely that the cessation of star formation will not disrupt a galaxy's late-type morphology. Our observations at $z = 1.6$ may be due to this same affect: differences we see between field galaxies and those in the outskirts of the cluster may be due to an earlier formation of dark matter halos in regions of high density. Bell et al. (2012) studied galaxies over a large range of redshift in the CANDELS UDS field, finding the $z \sim 1.6$ redshift slice to contain a high local number density of galaxies (presumably many groups). There are more quiescent galaxies with low Sérsic indices in this redshift slice than are seen in other slices. This reinforces the notion that quiescent galaxies with low Sérsic indices are the result of environment processes.

If the environment of the cluster does suppress gas accretion onto galaxies, then we naturally expect a higher quiescent fraction of galaxies in the vicinity of the cluster. We test this using the fraction of quiescent galaxies, f_Q, which is the ratio of the number of quiescent galaxies to the total number of galaxies. Taking galaxies with stellar mass $>2 \times 10^{10}\,M_\odot$ from the full UDS sample at the redshift of the cluster, we estimate an intrinsic quiescent fraction of $f_Q = 0.53$. This is consistent with the measurements from Quadri et al. (2012) considering differences in redshift binning, and in the measurements of the internal colors (see discussion in Section 2, Quadri et al. 2012; Brammer et al. 2009).

Figure 9 shows f_Q as a function of projected distance from the center of the cluster. The figure also shows the probability of obtaining the expected f_Q value for a binomial distribution given the numbers of galaxies in each bin. Galaxies within 1 Mpc show an enhancement in the quiescent fraction, with $f_Q = 0.62$–1.0. Using a binomial distribution, this is significant with $p = 0.033$ for all galaxies within 1 Mpc, about the 2σ level assuming a Gaussian distribution (and even higher significance, $p = 0.011$, considering the galaxies at 0.5–1 Mpc only).

There is evidence for an enhanced quiescent fraction in the cluster. At projected distances $R_{\rm proj} < 1$ Mpc, we observe a significant enhancement ($>2\sigma$) of the quiescent fraction (Figure 9). In the annulus 1 Mpc $< R_{\rm proj} <$ 1.5 Mpc, the galaxies

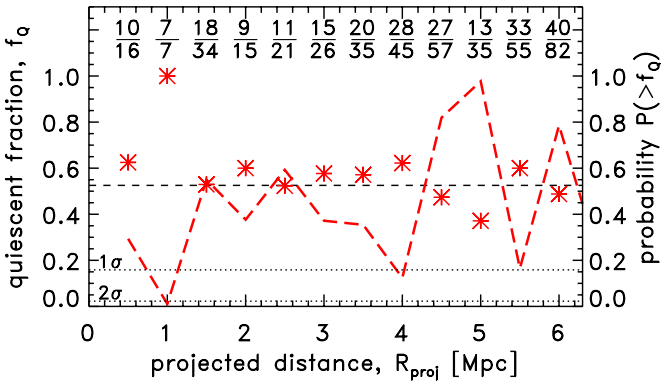

Figure 9. The fraction of quiescent galaxies, f_Q, as a function of projected distance from the center of the cluster. Galaxies have stellar mass $>2\times10^{10}\,M_\odot$. Each datum shows the ratio of the number of quiescent galaxies to the total in each bin of projected distance. This fraction is printed above each datum. The horizontal dashed line shows the quiescent fraction of all galaxies in the same (including both cluster and field samples), $f_Q = 0.52$. The long-dashed curve shows the probability of obtaining the measured fraction or greater assuming a binomial distribution assuming an intrinsic fraction of f_Q. The dotted lines show significance levels of 1σ and 2σ. The binomial probability is very dependent on the intrinsic fraction of f_Q, and the value we assume is a conservative upper limit for reasons in the text. At projected distances $R_{\rm proj} < 1$ Mpc, we observe a significant enhancement of the quiescent fraction, but this does not extend beyond 1 Mpc.

(A color version of this figure is available in the online journal.)

have a quiescent fraction that is consistent with the intrinsic fraction derived for all galaxies. As illustrated in Figure 4, the unchanging quiescent fraction from the annulus to the field results in a high number of star-forming galaxies in the annulus. We are unable to rule out the possibility that these star-forming galaxies result from contamination effects, and that the intrinsic quiescent fraction in the annulus is higher. It may also be possible that some processes acting to suppress star formation do not follow a spherically symmetric geometry (which we assume using an annulus of constant projected radius). Larger samples of cluster galaxies observed at large projected distances are needed to make more rigorous conclusions. Nevertheless, the evidence here is that the galaxies in the 1 Mpc $< R_{\rm proj} <$ 1.5 Mpc annulus have a quiescent fraction consistent with the field. This evidence disfavors (but does not exclude) the assembly bias scenario as this effect would likely exhibit an enhanced quiescent fraction in the near vicinity of the assembling cluster.

Our findings at $z = 1.6$ are similar to some studies at lower redshifts. Woo et al. (2012) show that at $z \sim 0$–0.2 and fixed stellar mass, the fraction of quiescent satellite galaxies is strongly dependent on the projected distance from the center of the parent halo, and that the fraction of "quenched" galaxies is enhanced out to projected distances of $\simeq 1.5\,R_{\rm vir}$ around massive halos ($M_h \sim 10^{14.5}\,M_\odot$). Weinmann et al. (2006) reach similar conclusions. Wetzel et al. (2011) similarly find that the fraction of quenched galaxies that are centrals in their halos is higher and deviates significantly from field values within $2 \times R_{\rm vir}$, but at larger clustercentric distances there is no indication that the environment has any effect on the star-formation in galaxies. Depending on the size of the virial radius of the cluster (upper limit of $R_{\rm vir} \simeq 0.9$ Mpc, see above), it appears that the quiescent fraction is enhanced out to distances of $\approx 1\,R_{\rm vir}$. Interestingly, the enhanced quiescent fraction does not extend to projected distances of 1–1.5 Mpc, which would be expected if field galaxies are being quenched as they are accreted into the cluster environment. A possible explanation is

that the galaxies in the annulus are in a group-sized dark matter halo(s), and may experience excess star formation (e.g., Tran et al. 2009) in addition to quenching that keeps the quiescent fraction approximately equivalent to the field value.

Another interesting system is the well-studied, X-ray luminous cluster XMMU J2235.3-2557 at a redshift of $z = 1.39$ (Lidman et al. 2008; Strazzullo et al. 2010; Bauer et al. 2011b). The core of this highly evolved cluster exhibits a tight red sequence of galaxies (very similar to the cluster at $z = 1.62$ in our field) with little or no ongoing star formation. The cluster members on the outskirts on the other hand show greater diversity and a notable increase in [O II] emitters and galaxies, which may be hosts of dust-obscured star formation. There is also evidence for a "quenching radius" (located ∼200 kpc from the cluster core) within which star formation is rapidly truncated, possibly in relation to the hot, X-ray-emitting intracluster medium. Grützbauch et al. (2012) extend the study out to $\sim 1.5 R_{\rm vir}$ and find SFRs lower than typical values for field galaxies at the same redshift. It is noted that clusters detected due to their extended X-ray emission are more likely to be evolved structures than clusters detected by different methods. Observations of XMMU J2235.3-2557 are consistent with more advanced stages of the evolution proposed for the cluster studied here.

Therefore, our interpretation of the data is that environments of higher density, such as the forming cluster at $z = 1.62$, accelerate the morphological evolution and quiescent fraction of galaxies. Furthermore, the data show that the environment has two effects. First, Lotz et al. (2013) and Papovich et al. (2012) argue for an increased merger rate within the densest environments in order to account for the larger effective sizes of quiescent galaxies and the elevated number of faint companions observed. Second, here we argue that as galaxies enter the sphere of influence of the cluster, star formation must be suppressed in some galaxies in order to explain their quiescent colors and morphologies (Section 4.4). Theory predicts that the physical effects associated with the cluster could include gas-shock heating, as discussed above. Another possibility that cannot be rejected is that galaxies near the cluster may experience assembly bias as they compete for baryonic gas with the larger gravitational potential of the cluster. Furthermore, Quadri et al. (2012) observe an upturn in the fraction of quiescent galaxies for lower-mass galaxies in higher density regions in the same mass and redshift range where we observe the change in morphologies, adding further evidence that the environment has a strong effect on galaxies of moderate mass. Therefore, at $z = 1.6$, it appears that the environment has a stronger effect on moderate-mass galaxies (2×10^{10}–$9 \times 10^{10}\ M_{\odot}$), as it is these galaxies that exhibit the most difference in size and Sérsic index compared to similar galaxies in the field (although we note that this applies less to the most massive quiescent galaxies, which show very similar sizes in both the cluster and field; Papovich et al. 2012).

6. SUMMARY

To summarize, in this paper, we have studied the dependence of galaxy color, stellar mass, and morphology for galaxies on environment at $z = 1.6$ in the CANDELS/UDS field. This field contains *HST* near-infrared imaging over 9.′4 × 22.′0, corresponding to a projected physical area of 4.8 Mpc × 11.2 Mpc at $z = 1.6$. This field also contains a known galaxy overdensity (cluster) at this redshift (Papovich et al. 2010). We define a sample of cluster galaxies as those within 1.5 Mpc of the cluster center, and we define a sample of galaxies in the field as those further than 3.0 Mpc of the cluster center. We also find it useful to define a sample of galaxies in an annulus between $R_{\rm proj} = 1$–1.5 Mpc from the cluster center. Because we use the same suite of ground-based and space-based data to study the properties of the galaxies in our samples, our study is very homogenous. Any systematic biases affecting our data or analysis will be identical, and studies of the relative properties between the cluster and field samples will be robust.

We derive stellar masses, rest-frame colors, and SFRs using the broad suite of ground-based and *Spitzer* data. We quantify the morphology of the galaxies using GALFIT with the *HST*/F125W data to measure the effective radius, $r_{\rm eff}$, and Sérsic index, n, of all galaxies in our samples. In both the cluster and field, half of the bulge-dominated galaxies ($n > 2$) reside on the red sequence of the color–magnitude diagram, and most disk-dominated galaxies ($n < 2$) reside in the blue cloud associated with star-forming galaxies. Applying the WMW statistical test to field and cluster galaxies, we derive some evidence that the cluster galaxies have redder rest-frame $U - B$ colors and higher stellar masses compared to the field. Star-forming galaxies in both the cluster and field show no significant differences in their morphologies. In contrast, there is evidence that quiescent galaxies in the cluster have larger median effective radii, $r_{\rm eff,med}^{\rm cluster} = 2.0$ kpc, and smaller Sérsic indices, $n_{\rm med}^{\rm cluster} = 2.6$, compared to the field, which have $r_{\rm eff,med}^{\rm field} = 1.4$ kpc and $n_{\rm med}^{\rm field} = 3.3$.

The differences in morphology are larger when comparing quiescent galaxies in an annulus defined by clustercentric distances 1 Mpc $< R_{\rm proj} <$ 1.5 Mpc to the other quiescent galaxies. The quiescent galaxies in this annulus have median $n_{\rm med}^{\rm 1-1.5\,Mpc} = 2.1$ and $r_{\rm reff,med}^{\rm 1-1.5\,Mpc} = 2.7$ kpc, more consistent with the morphologies of the star-forming galaxies. We find that the Sérsic index generally correlates with rest-frame $U - V$ color, such that the majority of red, quiescent galaxies have higher Sérsic indices ($n > 2$), consistent with the findings of Bell et al. (2012). However, a high fraction (≈50%) of the quiescent galaxies in the 1 Mpc $< R_{\rm proj} <$ 1.5 Mpc annulus have $n < 2$ compared to only <15% of quiescent galaxies overall. We argue that these galaxies have been processed under the influence of the cluster environment, and the evidence favors models where gas accretion onto these galaxies is suppressed.

We argue that the primary channel for the evolution of galaxies at $z = 1.6$ depends on the mass of the galaxy, as the galaxies in both the cluster and field show weak differences in their masses, sSFRs, and rest-frame $U - B$ colors.

Our results also show that the environment has some role in the morphological evolution of galaxies at $z = 1.6$. These differences are seen in the cluster as a lack of "compact" quiescent galaxies observed in the field (see also, Papovich et al. 2012). The quiescent cluster galaxies also have lower Sérsic indices compared to the field, and this is especially true for the quiescent galaxies in the annulus of 1–1.5 Mpc from the cluster. The change in galaxy properties in this annulus is especially interesting as these clustercentric distances are greater than estimates of the virial radius, which have an upper limit of 0.9 Mpc from dynamical and X-ray constraints (see Papovich et al. 2010 and Pierre et al. 2011). Taken together, we argue that the environment influences star-forming galaxies as they enter the sphere of influence of the cluster at ∼2 times the virial radius, and that this may affect more strongly the moderate-mass galaxies. This is consistent with expectations from theory, including effects from strangulation, preprocessing by groups, or assembly bias. Our data favors a scenario dominated by

Table 2
Summary of GALFIT Tests for *HST* WFC3 F125W Data

Output Magnitude	r_{out} Range (kpc)	n_{out} Range	$S_{BI}[(r_{out} - r_{in})/r_{in}]$	$S_{BI}[(n_{out} - n_{in})/n_{in}]$
20.5 ± 0.25	0–0.75	<1	0.002	0.005
		1–2.5	0.003	0.010
		>2.5	0.010	0.016
	1.0 ± 0.25	<1	0.002	0.004
		1–2.5	0.006	0.009
		>2.5	0.018	0.018
	1.5 ± 0.25	<1	0.004	0.005
		1–2.5	0.009	0.012
		>2.5	0.024	0.020
	2.0 ± 025	<1	0.005	0.005
		1–2.5	0.012	0.013
		>2.5	0.031	0.021
21.0 ± 0.25	0–0.75	<1	0.003	0.008
		1–2.5	0.005	0.018
		>2.5	0.017	0.026
	1.0 ± 0.25	<1	0.004	0.007
		1–2.5	0.009	0.015
		>2.5	0.031	0.031
	1.5 ± 0.25	<1	0.005	0.008
		1–2.5	0.015	0.020
		>2.5	0.044	0.034
	2.0 ± 0.25	<1	0.008	0.010
		1–2.5	0.019	0.020
		>2.5	0.065	0.044
21.5 ± 0.25	0–0.75	<1	0.005	0.012
		1–2.5	0.009	0.026
		>2.5	0.025	0.041
	1.0 ± 0.25	<1	0.006	0.010
		1–2.5	0.017	0.028
		>2.5	0.046	0.046
	1.5 ± 0.25	<1	0.010	0.015
		1–2.5	0.025	0.033
		>2.5	0.067	0.049
	2.0 ± 0.25	<1	0.013	0.015
		1–2.5	0.031	0.035
		>2.5	0.101	0.068
22.0 ± 0.25	0–0.75	<1	0.006	0.017
		1–2.5	0.015	0.042
		>2.5	0.048	0.078
	1.0 ± 0.25	<1	0.011	0.017
		1–2.5	0.025	0.040
		>2.5	0.059	0.065
	1.5 ± 0.25	<1	0.015	0.023
		1–2.5	0.036	0.048
		>2.5	0.086	0.071
	2.0 ± 0.25	<1	0.017	0.027
		1–2.5	0.053	0.058
		>2.5	0.256	0.158
22.5 ± 0.25	0–0.75	<1	0.014	0.030
		1–2.5	0.024	0.065
		>2.5	0.068	0.109
	1.0 ± 0.25	<1	0.018	0.022
		1–2.5	0.042	0.065
		>2.5	0.113	0.106
	1.5 ± 0.25	<1	0.023	0.034
		1–2.5	0.056	0.070
		>2.5	0.140	0.120
	2.0 ± 0.25	<1	0.031	0.047
		1–2.5	0.087	0.090
		>2.5	1.033	0.643
23.0 ± 0.25	0–0.75	<1	0.018	0.047
		1–2.5	0.038	0.092
		>2.5	0.095	0.161

Table 2
(Continued)

Output Magnitude	r_{out} Range (kpc)	n_{out} Range	$S_{BI}[(r_{out} - r_{in})/r_{in}]$	$S_{BI}[(n_{out} - n_{in})/n_{in}]$
	1.0 ± 0.25	<1	0.027	0.039
		1–2.5	0.063	0.106
		>2.5	0.152	0.161
	1.5 ± 0.25	<1	0.036	0.051
		1–2.5	0.089	0.110
		>2.5	0.222	0.196
	2.0 ± 0.25	<1	0.053	0.070
		1–2.5	0.129	0.135
		>2.5	3.571	0.881
23.5 ± 0.25	0–0.75	<1	0.033	0.074
		1–2.5	0.056	0.154
		>2.5	0.153	0.253
	1.0 ± 0.25	<1	0.044	0.066
		1–2.5	0.089	0.148
		>2.5	0.213	0.223
	1.5 ± 0.25	<1	0.063	0.074
		1–2.5	0.116	0.161
		>2.5	0.275	0.231
	2.0 ± 0.25	<1	0.093	0.094
		1–2.5	0.200	0.202
		>2.5	3.360	1.019
24.0 ± 0.25	0–0.75	<1	0.060	0.132
		1–2.5	0.108	0.273
		>2.5	0.186	0.301
	1.0 ± 0.25	<1	0.071	0.098
		1–2.5	0.138	0.251
		>2.5	0.332	0.308
	1.5 ± 0.25	<1	0.086	0.123
		1–2.5	0.194	0.285
		>2.5	0.384	0.359
	2.0 ± 0.25	<1	0.132	0.189
		1–2.5	0.273	0.305
		>2.5	3.243	0.940

strangulation, however, the other two possibilities cannot be excluded.

As a final word, it is unknown if our results are extendable to all quiescent galaxies in different environments at $z = 1.6$, including better statistics on group environments. Our results are based on a single forming galaxy cluster at $z \sim 1.6$, and even with the large CANDELS dataset, we have morphological information from *HST* for fewer than 100 quiescent galaxies at this redshift. Clearly, larger samples of galaxies at this (and other) redshifts are required to generalize these results and to improve (or refute) the significance of the differences in morphology we observe here. Such tests will be possible using the full CANDELS dataset as well as other *HST* studies in fields of high redshift clusters.

We wish to thank the members of the CANDELS team for their contributions, and we thank L. Macri and R. Quadri for stimulating discussions and helpful comments. We also wish to thank the anonymous referee for comments and suggestions that improved the quality and clarity of this work. This work is based on observations taken by the CANDELS Multi-Cycle Treasury Program with the NASA/ESA *HST*, which is operated by the Association of Universities for Research in Astronomy, Inc., under NASA contract NAS5-26555. This work is supported by *HST* program No. GO-12060. Support for Program No. GO-12060 was provided by NASA through a grant from the Space Telescope Science Institute, which is operated by the Association of Universities for Research in Astronomy, Incorporated, under NASA contract NAS5-26555. This work is based on observations made with the *Spitzer Space Telescope*, which is operated by the Jet Propulsion Laboratory, California Institute of Technology. This work is based in part on data obtained as part of the UKIRT Infrared Deep Sky Survey. M.C.C. acknowledges support provided by NASA through Hubble Fellowship grant No. HF-51269.01-A, awarded by the Space Telescope Science Institute, which is operated by the Association of Universities for Research in Astronomy, Inc., for NASA, under contract NAS 5-26555. M.C.C. also acknowledges support from the Southern California Center for Galaxy Evolution, a multi-campus research program funded by the University of California Office of Research. D.C. acknowledges receipt of a QEII Fellowship from the Australian Government. We acknowledge generous support from the George P. and Cynthia Woods Institute for Fundamental Physics and Astronomy.

APPENDIX

GALFIT TESTS

In order to determine to which magnitude we can reliably extract structural parameters of a galaxy using GALFIT, we performed a series of simulations. Galaxy models were created

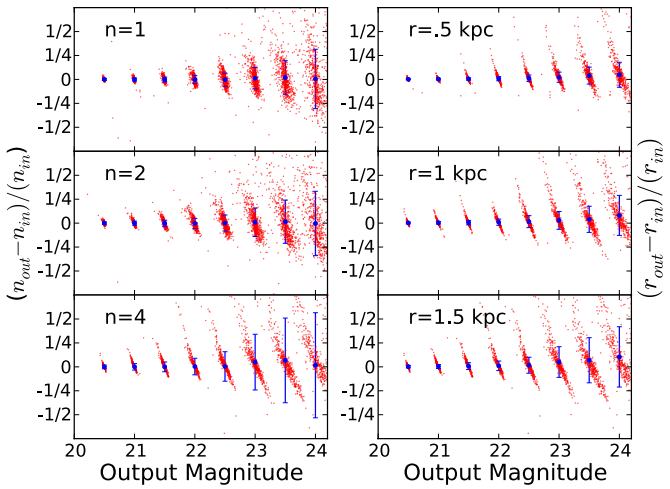

Figure 10. The GALFIT output magnitude vs. fractional difference in Sérsic index (left panel) and effective radius (right panel) between input and output values. The blue points show the median values, the error bars depict the biweighted scale (S_{BI}) as described in Beers et al. (1990). The points are placed in half magnitude wide bins with the center of the first bin at 20.5. The panels are separated vertically by Sérsic indices and effective radii values (respectively) used as input in our simulations. Note that because each panel is marginalized over the other parameter (e.g., $n = 1$ plot contains all $r_{\rm eff}$), this plot is not directly comparable to Table 2. Note also that the tendency for datapoints to be arranged in diagonal lines is due to the fact that input magnitudes were chosen at 0.5 mag steps. This is similar to the simulations of Häussler et al. (2007).

(A color version of this figure is available in the online journal.)

by running GALFIT with all fitted parameters (such as effective radius, Sérsic index, and magnitude) fixed to chosen values. The models were then inserted randomly into the *HST* F125W image, avoiding the edge and extreme proximity or overlap with existing objects. Then, GALFIT was run on these simulated galaxies embedded in our data in an attempt to recover the known values. The input models tested span a range of Sérsic indices, effective radii, and magnitudes typical of galaxies in our sample. The output values from these tests were then separated into bins 0.5 mag in size and the robust median and biweighted scale (as described in Beers et al. 1990) were computed for various input parameters. The results are summarized in Table 2 and plotted in Figure 10. As previously stated, our analysis of these simulations showed that the recovered effective radii are accurate to better than 40% and the Sérsic indices to better than 25% for galaxies with $r_{\rm eff} = 2$ kpc and $n = 4$ with magnitude m(F125W) = 24 mag, near the stellar-mass limit of our sample ($2 \times 10^{10}\ M_{\odot}$). Galaxies of this type are among the most difficult to fit: the effective radius and Sérsic index are highly covariant. Uncertainties are significantly lower for more disk-like and brighter sources (as shown in Table 2).

REFERENCES

Abadi, M. G., Moore, B., & Bower, R. G. 1999, MNRAS, 308, 947
Bahe, Y. M., McCarthy, I. G., Balogh, M. L., & Font, A. S. 2012, arXiv:1210.8407
Baldry, I. K., Balogh, M. L., Bower, R. G., et al. 2006, MNRAS, 373, 469
Balogh, M. L., Navarro, J. F., & Morris, S. L. 2000, ApJ, 540, 113
Barden, M., Häußler, B., Peng, C. Y., McIntosh, D. H., & Guo, Y. 2012, MNRAS, 2576
Bauer, A. E., Conselice, C. J., Pérez-González, P. G., et al. 2011a, MNRAS, 417, 289
Bauer, A. E., Grützbauch, R., Jørgensen, I., Varela, J., & Bergmann, M. 2011b, MNRAS, 411, 2009
Beers, T. C., Flynn, K., & Gebhardt, K. 1990, AJ, 100, 32
Behroozi, P. S., Wechsler, R. H., & Conroy, C. 2013, ApJL, 762, L31
Bell, E. F., van der Wel, A., Papovich, C., et al. 2012, ApJ, 753, 167
Birnboim, Y., & Dekel, A. 2003, MNRAS, 345, 349
Birnboim, Y., Dekel, A., & Neistein, E. 2007, MNRAS, 380, 339
Blakeslee, J. P., Franx, M., Postman, M., et al. 2003, ApJL, 596, L143
Blakeslee, J. P., Holden, B. P., Franx, M., et al. 2006, ApJ, 644, 30
Blanton, M. R., Eisenstein, D., Hogg, D. W., Schlegel, D. J., & Brinkmann, J. 2005, ApJ, 629, 143
Brammer, G. B., van Dokkum, P. G., & Coppi, P. 2008, ApJ, 686, 1503
Brammer, G. B., Whitaker, K. E., van Dokkum, P. G., et al. 2009, ApJL, 706, L173
Bruzual, G., & Charlot, S. 2003, MNRAS, 344, 1000
Calzetti, D., Armus, L., Bohlin, R. C., et al. 2000, ApJ, 533, 682
Chuter, R. W., Almaini, O., Hartley, W. G., et al. 2011, MNRAS, 413, 1678
Cooper, M. C., Gallazzi, A., Newman, J. A., & Yan, R. 2010, MNRAS, 402, 1942
Cooper, M. C., Griffith, R. L., Newman, J. A., et al. 2011, MNRAS, 419, 3018
Cooper, M. C., Newman, J. A., Coil, A. L., et al. 2007, MNRAS, 376, 1445
Cooper, M. C., Newman, J. A., Weiner, B. J., et al. 2008, MNRAS, 383, 1058
Croton, D. J., Gao, L., & White, S. D. M. 2007, MNRAS, 374, 1303
Croton, D. J., Springel, V., White, S. D. M., et al. 2006, MNRAS, 365, 11
Cucciati, O., Iovino, A., Kovač, K., et al. 2010, A&A, 524, A2
Cuesta, A. J., Prada, F., Klypin, A., & Moles, M. 2008, MNRAS, 389, 385
Daddi, E., Dickinson, M., Morrison, G., et al. 2007, ApJ, 670, 156
Dekel, A., & Birnboim, Y. 2006, MNRAS, 368, 2
Dekel, A., Birnboim, Y., Engel, G., et al. 2009, Natur, 457, 451
Dressler, A. 1980, ApJ, 236, 351
Elbaz, D., Daddi, E., Le Borgne, D., et al. 2007, A&A, 468, 33
Gao, L., Springel, V., & White, S. D. M. 2005, MNRAS, 363, L66
Grogin, N. A., Kocevski, D. D., Faber, S. M., et al. 2011, ApJS, 197, 35
Grützbauch, R., Bauer, A. E., Jørgensen, I., & Varela, J. 2012, MNRAS, 423, 3652
Grützbauch, R., Conselice, C. J., Bauer, A. E., et al. 2011a, MNRAS, 418, 938
Grützbauch, R., Conselice, C. J., Varela, J., et al. 2011b, MNRAS, 411, 929
Gunn, J. E., & Gott, J. R., III. 1972, ApJ, 176, 1
Guo, Y., McIntosh, D. H., Mo, H. J., et al. 2009, MNRAS, 398, 1129
Haas, M. R., Schaye, J., & Jeeson-Daniel, A. 2011, MNRAS, 419, 2133
Hansen, S. M., Sheldon, E. S., Wechsler, R. H., & Koester, B. P. 2009, ApJ, 699, 1333
Häussler, B., McIntosh, D. H., Barden, M., et al. 2007, ApJS, 172, 615
Hogg, D. W., Blanton, M. R., Brinchmann, J., et al. 2004, ApJL, 601, L29
Hogg, D. W., Blanton, M. R., Eisenstein, D. J., et al. 2003, ApJL, 585, L5
Holden, B. P., Blakeslee, J. P., Postman, M., et al. 2005, ApJ, 626, 809
Homeier, N. L., Demarco, R., Rosati, P., et al. 2005, ApJ, 621, 651
Kauffmann, G., White, S. D. M., Heckman, T. M., et al. 2004, MNRAS, 353, 713
Kocevski, D. D., Lemaux, B. C., Lubin, L. M., et al. 2011, ApJ, 736, 38
Koekemoer, A. M., Faber, S. M., Ferguson, H. C., et al. 2011, ApJS, 197, 36
Kravtsov, A. V., Nagai, D., & Vikhlinin, A. A. 2005, ApJ, 625, 588
Kriek, M., van Dokkum, P. G., Franx, M., et al. 2006, ApJL, 649, L71
Krist, J. 1995, in ASP Conf. Ser. 77, Astronomical Data Analysis Software and Systems IV, ed. R. A. Shaw, H. E. Payne, & J. J. E. Hayes (San Francisco, CA: ASP), 349
Lidman, C., Rosati, P., Tanaka, M., et al. 2008, A&A, 489, 981
Lotz, J. M., Papovich, C., Faber, S. M., et al. 2013, ApJ, submitted (arXiv:1110.3821)
Mann, H. B., & Whitney, D. R. 1947, The Annals of Mathematical Statistics, 18, 50
McGee, S. L., Balogh, M. L., Bower, R. G., Font, A. S., & McCarthy, I. G. 2009, MNRAS, 400, 937
Mei, S., Holden, B. P., Blakeslee, J. P., et al. 2009, ApJ, 690, 42
Moore, B., Katz, N., Lake, G., Dressler, A., & Oemler, A. 1996, Natur, 379, 613
Muldrew, S. I., Croton, D. J., Skibba, R. A., et al. 2012, MNRAS, 419, 2670
Navarro, J. F. 1990, MNRAS, 242, 311
Noeske, K. G., Weiner, B. J., Faber, S. M., et al. 2007, ApJL, 660, L43
Oke, J. B., & Gunn, J. E. 1983, ApJ, 266, 713
Papovich, C., Bassett, R., Lotz, J. M., et al. 2012, ApJ, 750, 93
Papovich, C., Momcheva, I., Willmer, C. N. A., et al. 2010, ApJ, 716, 1503
Patel, S. G., Holden, B. P., Kelson, D. D., Illingworth, G. D., & Franx, M. 2009, ApJL, 705, L67
Peng, C. Y., Ho, L. C., Impey, C. D., & Rix, H. 2002, AJ, 124, 266
Peng, Y.-j., Lilly, S. J., Kovač, K., et al. 2010, ApJ, 721, 193
Pierre, M., Clerc, N., Maughan, B., et al. 2011, arXiv:1109.6194
Pierre, M., Clerc, N., Maughan, B., et al. 2012, A&A, 540, A4
Poggianti, B. M., Desai, V., Finn, R., et al. 2008, ApJ, 684, 888
Postman, M., Franx, M., Cross, N. J. G., et al. 2005, ApJ, 623, 721
Postman, M., & Geller, M. J. 1984, ApJ, 281, 95

Quadri, R. F., Williams, R. J., Franx, M., & Hildebrandt, H. 2012, ApJ, 744, 88
Read, J. I., Wilkinson, M. I., Evans, N. W., Gilmore, G., & Kleyna, J. T. 2006, MNRAS, 366, 429
Rudnick, G. H., Tran, K.-V., Papovich, C., Momcheva, I., & Willmer, C. 2012, ApJ, 755, 14
Santos, J. S., Rosati, P., Gobat, R., et al. 2009, A&A, 501, 49
Sersic, J. L. 1968, Atlas de Galaxias Australes (Cordoba, Argentina: Observatorio Astronomico)
Skibba, R. A., Bamford, S. P., Nichol, R. C., et al. 2009, MNRAS, 399, 966
Strazzullo, V., Rosati, P., Pannella, M., et al. 2010, A&A, 524, A17
Tasca, L. A. M., Kneib, J.-P., Iovino, A., et al. 2009, A&A, 503, 379
Thomas, D., Maraston, C., Bender, R., & Mendes de Oliveira, C. 2005, ApJ, 621, 673
Tran, K., Papovich, C., Saintonge, A., et al. 2010, ApJL, 719, L126
Tran, K., Saintonge, A., Moustakas, J., et al. 2009, ApJ, 705, 809
Tran, K., van Dokkum, P., Franx, M., et al. 2005, ApJL, 627, L25
van der Wel, A. 2008, ApJL, 675, L13
van der Wel, A., Bell, E. F., Häussler, B., et al. 2012, ApJS, 203, 24
van der Wel, A., Holden, B. P., Zirm, A. W., et al. 2008, ApJ, 688, 48
Wechsler, R. H., Zentner, A. R., Bullock, J. S., Kravtsov, A. V., & Allgood, B. 2006, ApJ, 652, 71
Weinmann, S. M., Kauffmann, G., van den Bosch, F. C., et al. 2009, MNRAS, 394, 1213
Weinmann, S. M., van den Bosch, F. C., Yang, X., & Mo, H. J. 2006, MNRAS, 366, 2
Wetzel, A. R., Tinker, J. L., & Conroy, C. 2011, arXiv:1107.5311
White, S. D. M., & Rees, M. J. 1978, MNRAS, 183, 341
Williams, R. J., Quadri, R. F., Franx, M., van Dokkum, P., & Labbé, I. 2009, ApJ, 691, 1879
Wilman, D. J., Erwin, P., De Lucia, G., Fontanot, F., & Monaco, P. 2011, in The Origin of the Morphology-Density Relation, ed. I. Ferreras & A. Pasquali (Berlin: Springer), 215
Woo, J., Dekel, A., Faber, S. M., et al. 2012, arXiv:1203.1625
Wuyts, S., Forster Schreiber, N. M., van der Wel, A., et al. 2011, ApJ, 742, 96
Wuyts, S., Labbé, I., Franx, M., et al. 2007, ApJ, 655, 51
Zirm, A. W., Toft, S., & Tanaka, M. 2011, ApJ, 744, 181